J|A|C|S
ARTICLES
Published on Web 10/17/2006

Mechanistic Borderline between One-Step Hydrogen Transfer and Sequential Transfers of Electron and Proton in Reactions of NADH Analogues with Triplet Excited States of Tetrazines and $Ru(bpy)_3^{2+*}$

Junpei Yuasa and Shunichi Fukuzumi*

Contribution from the Department of Material and Life Science, Graduate School of Engineering, Osaka University, SORST, Japan Science and Technology Agency (JST), Suita, Osaka 565-0871, Japan

Received January 20, 2006; E-mail: fukuzumi@chem.eng.osaka-u.ac.jp

Abstract: Efficient energy transfer from $Ru(bpy)_3^{2+*}$ (bpy = 2,2′-bipyridine, * denotes the excited state) to 3,6-disubstituted tetrazines [R_2Tz: R = Ph (Ph_2Tz), 2-chlorophenyl [$(ClPh)_2Tz$], 2-pyridyl (Py_2Tz)] occurs to yield the triplet excited states of tetrazines ($^3R_2Tz^*$), which have longer lifetimes and higher oxidizing ability as compared with those of $Ru(bpy)_3^{2+*}$. The dynamics of hydrogen-transfer reactions from NADH (dihydronicotinamide adenine dinucleotide) analogues has been examined in detail using $^3R_2Tz^*$ by laser flash photolysis measurements. Whether formal hydrogen transfer from NADH analogues to $^3R_2Tz^*$ proceeds via a one-step process or sequential electron and proton transfer processes is changed by a subtle difference in the electron donor ability and the deprotonation reactivity of the radical cations of NADH analogues as well as the electron-acceptor ability of $^3R_2Tz^*$ and the protonation reactivity of $R_2Tz^{\bullet-}$. In the case of $^3Ph_2Tz^*$, which is a weaker electron acceptor than the other tetrazine derivatives [$(ClPh)_2Tz$; Py_2Tz], direct one-step hydrogen transfer occurs from 10-methyl-9,10-dihydroacridine ($AcrH_2$) to $^3Ph_2Tz^*$ without formation of the radical cation ($AcrH_2^{\bullet+}$). The rate constant of the direct hydrogen transfer from $AcrH_2$ to $^3Ph_2Tz^*$ is larger than that expected from the Gibbs energy relation for the rate constants of electron transfer from various electron donors to $^3Ph_2Tz^*$, exhibiting the primary deuterium kinetic isotope effect. On the other hand, hydrogen transfer from 9-isopropyl-10-methyl-9,10-dihydroacridine ($AcrHPr^i$) and 1-benzyl-1,4-dihydronicotinamide (BNAH) to $^3R_2Tz^*$ occurs via sequential electron and proton transfer processes, when both the radical cations and deprotonated radicals of NADH analogues are detected by the laser flash photolysis measurements.

Introduction

Hydrogen transfer from hydrogen donors (RH) to the triplet excited states of hydrogen acceptors ($^3A^*$), $RH + {}^3A^* \rightarrow R^\bullet + AH^\bullet$, is one of the most important and fundamental reactions in organic photochemistry.[1−6] There are two possible reaction pathways in hydrogen transfer to the triplet state species: one is one-step hydrogen transfer, and the other is sequential electron and proton transfer (Scheme 1).[7−15] The one-step mechanism

Scheme 1

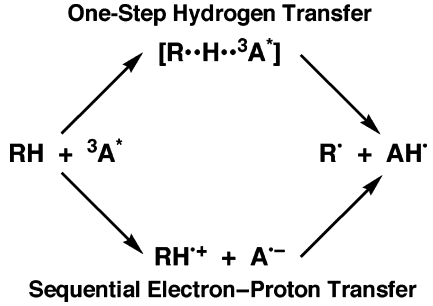

means that the hydrogen-transfer reaction occurs without an intermediate when an electron and proton are transferred at the same time. Such reactions are generally regarded as proton-coupled electron transfer (PCET), and the definition of PCET encompasses both hydrogen atom transfer (HAT) and concerted electron and proton transfer.[15,16] It is to be contrasted with the

(1) (a) Wagner, P. J. *Top. Curr. Chem.* **1976**, *66*, 1. (b) Wagner, P. J.; Park, B. S. *Org. Photochem.* **1991**, *11*, 227. (c) Wagner, P. J. *Acc. Chem. Res.* **1971**, *4*, 168.
(2) (a) Turro, N. J. In *Modern Molecular Photochemistry*; Benjamin/Cummings: Menlo Park, CA, 1978; pp 137−146. (b) Turro, N. J.; Dalton, J. C.; Dawaes, K.; Farrington, G.; Hautala, R.; Morton, D.; Niemczyk, M.; Schore, N. *Acc. Chem. Res.* **1972**, *5*, 92.
(3) Zimmerman, H. E. *Adv. Photochem.* **1963**, *1*, 183.
(4) (a) Gilbert, A.; Baggott, J. In *Essentials of Molecular Photochemistry*; CRC Press: Boston, 1991; pp 302−328. (b) Schuster, D. I.; Karp, P. B. *J. Photochem.* **1980**, *12*, 333.
(5) Monroe, B. M.; Weed, G. C. *Chem. Rev.* **1993**, *93*, 435.
(6) Cohen, S. G.; Parola, A.; Parsons, G. H. *Chem. Rev.* **1973**, *73*, 141.
(7) (a) Wagner, P. J.; Truman, R. J.; Puchalski, A. E.; Wake, R. *J. Am. Chem. Soc.* **1986**, *108*, 7727. (b) Wagner, P. J.; Thomas, M. J.; Puchalski, A. E. *J. Am. Chem. Soc.* **1986**, *108*, 7739.
(8) Bockman, T. M.; Hubig, S. M.; Kochi, J. K. *J. Am. Chem. Soc.* **1998**, *120*, 2826.
(9) Canonica, S.; Hellrung, B.; Wirz, J. *J. Phys. Chem. A* **2000**, *104*, 1226.
(10) (a) Jones, G., II; Mouli, N. *J. Phys. Chem.* **1988**, *92*, 7174. (b) Jones, G., II; Mouli, N.; Haney, W. A.; Bergmark, W. R. *J. Am. Chem. Soc.* **1997**, *119*, 8788.
(11) Wong, S. K. *J. Am. Chem. Soc.* **1978**, *100*, 5488.
(12) Coenjarts, C.; Scaiano, J. C. *J. Am. Chem. Soc.* **2000**, *122*, 3635.

Chart 1

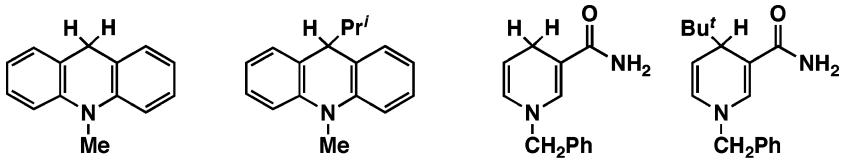

sequential pathway that involves mechanistically distinct electron transfer and proton transfer steps and thereby involves a detectable intermediate. There has been a long standing ambiguity as to the mechanistic borderline where a one-step hydrogen-transfer pathway is changed to a sequential electron and proton transfer pathway or vice versa.[7−15]

Among a variety of hydrogen donors, dihydronicotinamide adenine dinucleotide (NADH) and analogues have attracted particular interest, because NADH is the most important source of hydrogen and hydride ion in biological redox reactions.[17,18] If the hydrogen transfer from NADH and analogues to $^3A^*$ occurs in a one-step manner, $NAD^•$ and $AH^•$ would be the only detectable radical products. In the case of sequential electron and proton transfer, however, $NADH^{•+}$ and $A^{•-}$ would also be detected as the intermediates for the hydrogen-transfer reaction. The radical intermediates such as $NADH^{•+}$, $NAD^•$, and the corresponding analogues are involved in a variety of thermal and photoinduced electron-transfer reactions of NADH and analogues.[19−30] However, no systematic studies on the detection of $NADH^{•+}$, $NAD^•$, and the corresponding analogues have so far been performed in hydrogen-transfer reactions from NADH and analogues to the triplet excited states of hydrogen acceptors. Thus, the mechanistic borderline between one-step and sequential pathways in hydrogen-transfer reactions of NADH and analogues has yet to be clarified.

The triplet excited states of carbonyl compounds have been commonly used as reactive hydrogen acceptors because of the strong biradical character.[1−6,31] The one-reduced species of carbonyl compounds act as strong bases. In such a case, it would be very difficult to find the mechanistic borderline between one-step hydrogen transfer and sequential transfers of an electron and a proton because the subsequent proton-transfer step and net hydrogen transfer are generally too fast to detect any intermediate when sequential transfers of electron and proton occur.[7−15,32] Thus, the appropriate choice of the triplet excited state, which has relatively mild radical character but strong oxidizing ability with weak basicity of the one-electron reduced species, is of primary importance to find the mechanistic borderline between the one-step hydrogen transfer and sequential transfers of electron and proton in hydrogen-transfer reactions.

We report herein the mechanistic borderline between a one-step hydrogen-transfer pathway and a sequential electron−proton-transfer pathway in hydrogen-transfer reactions from a series of NADH analogues (Chart 1) to the triplet excited states of tetrazines (Chart 2). 1,2,4,5-Tetrazines are known as electron-deficient 4π compounds containing a N═N double bond, which have been extensively utilized in inverse electron demanding Diels−Alder reactions for synthesis of a variety of valuable compounds.[33−35] With regard to the triplet excited states of tetrazines, we have found that the triplet excited states of

(13) (a) Schaefer, C. G.; Peters, K. S. *J. Am. Chem. Soc.* **1980**, *102*, 7566. (b) Peters, K. S.; Pang, E.; Rudzki, J. *J. Am. Chem. Soc.* **1982**, *104*, 5535. (c) Manring, L. E.; Peters, K. S. *J. Am. Chem. Soc.* **1985**, *107*, 6452. (d) Peters, K. S.; Cashin, A.; Timbers, P. *J. Am. Chem. Soc.* **2000**, *122*, 107. (e) Dreyer, J.; Peters, K. S. *J. Phys. Chem.* **1996**, *100*, 19412.
(14) (a) Sjodin, M.; Styring, S.; Wolpher, H.; Xu, Y.; Sun, L.; Hammarstrom, L. *J. Am. Chem. Soc.* **2005**, *127*, 3855. (b) Sjodin, M.; Styring, S.; Akermark, B.; Sun, L.; Hammarstrom, L. *J. Am. Chem. Soc.* **2000**, *122*, 3932.
(15) For reactions involving OH rather than CH substrates, initial proton transfer ($ROH + {}^3A^* \rightarrow RO^- + AH^+$) should also be included as a possible mechanism, see: Mayer, J. M. *Annu. Rev. Phys. Chem.* **2004**, *55*, 363.
(16) For various definitions and examples of PCET, see: (a) Mayer, J. M.; Rhile, I. J. *Biochim. Biophys. Acta* **2004**, *1655*, 51. (b) Cukier, R. I.; Nocera, D. G. *Annu. Rev. Phys. Chem.* **1998**, *49*, 337. (c) Kohen, A.; Klinman, J. P. *Acc. Chem. Res.* **1998,** *31*, 397. (d) Hammes-Schiffer, S. *Acc. Chem. Res.* **2001**, *34*, 273. (e) Stubbe, J.; Nocera, D. G.; Yee, C. S.; Chang, M. C. Y. *Chem. Rev.* **2003**, *103*, 2167. (f) Chang, C. J.; Chang, M. C. Y.; Damrauer, N. H.; Nocera, D. G. *Biochim. Biophys. Acta* **2004**, *1655*, 13. (g) Bryant, J. R.; Mayer, J. M. *J. Am. Chem. Soc.* **2003**, *125*, 10351. (h) Roth, J. P.; Yoder, J. C.; Won, T.-J.; Mayer, J. M. *Science* **2001**, *294*, 2524. (i) Isborn, C.; Hrovat, D. A.; Borden, W. T.; Mayer, J. M.; Carpenter, B. K. *J. Am. Chem. Soc.* **2005**, *127*, 5794. (j) Mayer, J. M.; Hrovat, D. A.; Thomas, J. L.; Borden, W. T. *J. Am. Chem. Soc.* **2002**, *124*, 11142.
(17) Stryer, L. *Biochemistry*, 3rd ed; Freeman: New York, 1988; Chapter 17.
(18) (a) Fukuzumi, S.; Tanaka, T. In *Photoinduced Electron Transfer*; Fox, M. A., Chanon, M., Eds.; Elsevier: Amsterdam, 1988; Part C, Chapter 10. (b) Fukuzumi, S. In *Advances in Electron-Transfer Chemistry*; Mariano, P. S., Ed.; JAI Press: Greenwich, CT, 1992; pp 67−175.
(19) Fukuzumi, S.; Koumitsu, S.; Hironaka, K.; Tanaka, T. *J. Am. Chem. Soc.* **1987**, *109*, 305.
(20) (a) Fukuzumi, S.; Inada, O.; Suenobu, T. *J. Am. Chem. Soc.* **2003**, *125*, 4808. (b) Fukuzumi, S.; Inada, O.; Suenobu, T. *J. Am. Chem. Soc.* **2002**, *124*, 14538.
(21) (a) Fukuzumi, S.; Okubo, K.; Okamoto, T. *J. Am. Chem. Soc.* **2002**, *124*, 14147. (b) Fukuzumi, S.; Fujii, Y.; Suenobu, T. *J. Am. Chem. Soc.* **2001**, *123*, 10191.
(22) Fukuzumi, S.; Ohkubo, K.; Tokuda, Y.; Suenobu, T. *J. Am. Chem. Soc.* **2000**, *122*, 4286.
(23) (a) Fukuzumi, S.; Tokuda, Y.; Kitano, T.; Okamoto, T.; Otera, J. *J. Am. Chem. Soc.* **1993**, *115*, 8960. (b) Fukuzumi, S.; Kitano, T.; Tanaka, T. *Chem. Lett.* **1989**, 1231.
(24) (a) Gebicki, J.; Marcinek, A.; Zielonka, J. *Acc. Chem. Res.* **2004**, *37*, 379. (b) Zielonka, J.; Marcinek, A.; Adamus, J.; Gebicki, J. *J. Phys. Chem. A* **2003**, *107*, 9860. (c) Gebicki, J.; Marcinek, A.; Adamus, J.; Paneth, P.; Rogowski, J. *J. Am. Chem. Soc.* **1996**, *118*, 691. (d) Marcinek, A.; Adamus, J.; Huben, K.; Gebicki, J.; Bartczak, T. J.; Bednarek, P.; Bally, T. *J. Am. Chem. Soc.* **2000**, *122*, 437.
(25) (a) Pestovsky, O.; Bakac, A.; Espenson, J. H. *J. Am. Chem. Soc.* **1998**, *120*, 13422. (b) Pestovsky, O.; Bakac, A.; Espenson, J. H. *Inorg. Chem.* **1998**, *37*, 1616.
(26) (a) Tanner, D. D.; Kharrat, A.; Oumar-Mahamat, H. *Can. J. Chem.* **1990**, *68*, 11662. (b) Tanner, D. D.; Kharrat, A. *J. Org. Chem.* **1988**, *53*, 1646. (c) Liu, Y.-C.; Li, B.; Guo, Q.-X. *Tetrahedron* **1995**, *51*, 9671.
(27) Carlson, B. W.; Miller, L. L. *J. Am. Chem. Soc.* **1985**, *107*, 479.
(28) (a) Zhu, X.-Q.; Yang, Y.; Zhang, M.; Cheng, J.-P. *J. Am. Chem. Soc.* **2003**, *125*, 15298. (b) Zhu, X.-Q.; Cao, L.; Liu, Y.; Yang, Y.; Lu, J.-Y.; Wang, J.-S.; Cheng, J.-P. *Chem.—Eur. J.* **2003**, *9*, 3937. (c) Zhu, X.-Q.; Li, H.-R.; Li, Q.; Ai, T.; Lu, J.-Y.; Yang, Y.; Cheng, J.-P. *Chem.—Eur. J.* **2003**, *9*, 871. (d) Cheng, J.-P.; Lu, Y.; Zhu, X.-Q.; Mu, L. *J. Org. Chem.* **1998**, *63*, 6108. (e) Cheng, J.-P.; Handoo, K. L.; Xue, J.; Parker, V. D. *J. Org. Chem.* **1993**, *58*, 5050.
(29) Fukuzumi, S.; Yuasa, J.; Suenobu, T. *J. Am. Chem. Soc.* **2002**, *124*, 12566.
(30) Hydrogen-transfer reactions of NADH analogues have been also examined; see: (a) Fukuzumi, S.; Tokuda, Y.; Chiba, Y.; Greci, L.; Carloni, P.; Damiani, E. *J. Chem. Soc., Chem. Commun.* **1993**, 1575. (b) Matsuo, T.; Mayer, J. M. *Inorg. Chem.* **2005**, *44*, 2150.
(31) Singhal, N.; Koner, A. L.; Mal, P.; Venugopalan, P.; Nau, W. M.; Moorthy, J. N. *J. Am. Chem. Soc.* **2005**, *127*, 14375.
(32) Steric interaction is also an essential factor to determine the rate of hydrogen transfer; see: Tanko, J. M.; Friedline, R.; Suleman, N. K.; Castagnoli, N., Jr. *J. Am. Chem. Soc.* **2001**, *123*, 5808.

Chart 2

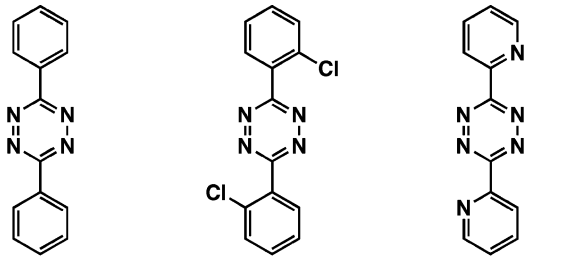

tetrazines, which have a relatively mild biradical character, are efficiently formed by photosensitization with Ru(bpy)$_3^{2+}$, although the direct photoexcitation of tetrazines affords no triplet excited state.[36,37]

We have previously reported the preliminary results on formation of ^{3}Ph$_2$Tz*.[38] The lifetimes and the oxidizing ability are much improved as compared with those of Ru(bpy)$_3^{2+*}$.[39,40] The change of mechanisms between a one-step hydrogen-transfer pathway and a sequential electron−proton-transfer pathway in the hydrogen-transfer reactions of NADH analogues with the triplet excited states of tetrazines depending on the type of NADH analogues and tetrazines is examined in full detail by the laser flash photolysis measurements.

Experimental Section

Materials. 3,6-Diphenyl-1,2,4,5-tetrazine (Ph$_2$Tz), 3,6-bis(2-chlorophenyl)-1,2,4,5-tetrazine [(ClPh)$_2$Tz], and 3,6-di-2-pyridyl-1,2,4,5-tetrazine (Py$_2$Tz) were obtained from Aldrich. Preparation of 10-methyl-9,10-dihydroacridine (AcrH$_2$) and the dideuterated compound (AcrD$_2$) was described previously.[19] 1-Benzyl-1,4-dihydronicotinamide (BNAH) was synthesized according to the literature.[19] The dideuterated compound, 1-benzyl-1,4-dihydro[4,4′-^{2}H$_2$] nicotinamide (BNAH-4,4′-d_2), was prepared from a monodeuterated compound (BNAH-4-d_1)[41] by three cycles of oxidation with *p*-chloranil in dimethyl formamide and reduction with dithionite in deuteriumoxide.[42] The 4-*tert*-butylated BNAH (4-*t*-BuBNAH) was prepared by a Grignard reaction with BNA$^+$Cl$^-$ and purified by recrystallization from ethanol.[20] 9-Isopropyl-10-methyl-9,10-dihydoacridine (AcrHPr^i) was prepared by the photoreduction of AcrH$^+$ClO$_4^-$ with Pr^{i}COOH in the presence of NaOH in H$_2$O−MeCN as reported previously.[23b] Tris(2,2′-bipyridyl)ruthenium(II) chloride hexahydrate [Ru(bpy)$_3$Cl$_2$·6H$_2$O] was obtained from Aldrich. Acetonitrile (MeCN) used as a solvent was purified and dried by the standard procedure.[43] Tetra-*n*-butylammonium perchlorate (TBAP) was purchased from Fluka Chemical Co., twice recrystallized from absolute ethanol, and dried in a vacuum at 45 °C prior to use. [^{2}H$_3$]acetonitrile (CD$_3$CN) was obtained from EURI SO-TOP, CEA, France.

Emission Quenching. Quenching experiments of the emission of Ru(bpy)$_3^{2+}$ by various electron donors were performed using a Shimadzu spectrofluorophotometer (RF-5000). The excitation wavelength of Ru(bpy)$_3^{2+}$ was 450 nm.[44] Typically, an MeCN solution was deaerated by argon purging for 8 min prior to measurements. Relative emission intensities were measured for MeCN solutions containing Ru(bpy)$_3^{2+}$ (4.6×10^{-5} M) with Ph$_2$Tz (1.0×10^{-5}−4.8×10^{-4} M). There was no change in the shape, but there was a change in the intensity of the emission spectrum by the addition of a quencher (A). The Stern−Volmer relationship (eq 1) was obtained for the ratio of the emission intensities and concentrations of quenchers. The

$$I_0/I = 1 + K_{SV}[A] \quad (1)$$

observed rate constants k_{EN} ($K_{SV}\tau^{-1}$) of energy transfer were obtained from the Stern−Volmer constants (K_{SV}) and the emission lifetime τ (850 ns) of Ru(bpy)$_3^{2+*}$ in deaerated MeCN at 298 K.[39]

Near-IR luminescence spectra of singlet oxygen were measured on a Hamamatsu Photonics R5509-72 photomultiplier under irradiation at 462 nm with use of a Cosmo System LVU-200S monochromator.

Cyclic Voltammetry. Cyclic voltammetry measurements were performed using an ALS electrochemical analyzer in deaerated MeCN containing 0.1 M Bu$_4$NClO$_4$ (TBAP) as the supporting electrolyte at 298 K. A conventional three-electrode cell was used with a platinum working electrode (surface area of 0.3 mm^2) and a platinum wire as the counter electrode. The Pt working electrode (BAS) was routinely polished with a BAS polishing alumina suspension and rinsed with acetone before use. The measured potentials were recorded with respect to the Ag/AgNO$_3$ (0.01 M) reference electrode. All potentials (vs Ag/Ag$^+$) were converted to values versus SCE by adding 0.29 V.[45] All electrochemical measurements were carried out under an atmospheric pressure of argon. Thin-layer spectroelectrochemical measurements were carried out with an optically transparent platinum thin-layer working electrode using a Hewlett-Packard model 8453 diode array spectrophotometer coupled with an EG&G model 173 universal programmer.

Laser Flash Photolysis. A deaerated MeCN solution containing Ru(bpy)$_3^{2+}$ and 3,6-disubstituted tetrazines (R$_2$Tz) was excited by a Nd:YAG laser (Continuum, SLII-10, 4−6 ns fwhm) at λ = 450 nm with the power of 8.6 mJ per pulse. The transient absorption spectra were measured using a continuous Xe lamp (150 W) and a photomultiplier tube (Hamamatsu 2949) as a probe light and a detector, respectively. The output from the photomultiplier tube was recorded with a digitizing oscilloscope (Tektronix, TDS3032, 300 MHz). The transient absorption spectra were recorded using fresh solutions in each laser excitation at 298 K.

(33) (a) Sauer, J. In *1,2,4,5-Tetrazines, in Comprehensive Heterocyclic Chemistry II*; Katritzky, A. R., Rees, C. W., Scriven, E. F., Eds.; Permagon Press: Oxford, 1996; Vol. 6, pp 901−957. (b) Sauer, J.; Bäuerlein, P.; Ebenbeck, W.; Schuster, J.; Sellner, I.; Sichert, H.; Stimmelmayr, H. *Eur. J. Org. Chem.* **2002**, 791.
(34) (a) Boger, D. L.; Hong, J. *J. Am. Chem. Soc.* **2001**, *123*, 8515. (b) Boger, D. L.; Schaum, R. P.; Garbaccio, R. M. *J. Org. Chem.* **1998**, *63*, 6329. (c) Boger, D. L.; Boyce, C. W.; Labroli, M. A.; Sehon, C. A.; Jin, Q. *J. Am. Chem. Soc.* **1999**, *121*, 54. (d) Miller, G. P.; Tetreau, M. C. *Org. Lett.* **2000**, *2*, 3091.
(35) Qian, W.; Chuang, S.-C.; Amador, R. B.; Jarrosson, T.; Sander, M.; Pieniazek, S.; Khan, S. I.; Rubin, Y. *J. Am. Chem. Soc.* **2003**, *125*, 2066.
(36) (a) Kavarnos G. J.; Turro, N. J. *Chem. Rev.* **1986**, *86*, 401. (b) Bock, C. R.; Connor, J. A.; Gutierrez, A. R.; Meyer, T. J.; Whitten, D. G.; Sullivan B. P.; Nagle, J. K. *J. Am. Chem. Soc.* **1979**, *101*, 4815. (c) Ballardini, R.; Varani, G.; Indelli, M. T.; Scandola, F.; Balzani. V. *J. Am. Chem. Soc.* **1978**, *100*, 7219.
(37) The phosphorescence can only be observed under specific conditions, such as in 1,2,4,5-tetrazine vapor, or mixed crystal at low temperature. In addition, unsubstituted 1,2,4,5-tetrazine is known to undergo efficient photochemical decomposition, breaking apart to 2HCN + N$_2$; see: (a) McDonald, J. R.; Brus, L. E. *J. Chem. Phys.* **1973**, *59*, 4966. (b) Hochstrasser, R. M.; King, D. S. *Chem. Phys.* **1974**, 5, 439. (c) Hochstrasser, R. M.; King, D. S. *J. Am. Chem. Soc.* **1975**, *97*, 4760.
(38) A part of preliminary results on formation of ^{3}Ph$_2$Tz* has appeared; see: Yuasa, J.; Fukuzumi, S. *Chem. Commun.* **2006**, 561.
(39) Ru(bpy)$_3^{2+}$ has proven to be the most versatile photosensitizer amongst a number of photosensitizers; see: Kavarnos G. J.; Turro, N. J. *Chem. Rev.* **1986**, *86*, 401. References 36c and 40.
(40) Bock, C. R.; Connor, J. A.; Gutierrez, A. R.; Meyer, T. J.; Whitten, D. G.; Sullivan B. P.; Nagle, J. K. *J. Am. Chem. Soc.* **1979**, *101*, 4815.
(41) (a) Anderson, A. G., Jr.; Berkelhammer, G. *J. Am. Chem. Soc.* **1958**, *80*, 992. (b) Mauzerall, D.; Westheimer, F. H. *J. Am. Chem. Soc.* **1955**, *77*, 2261.
(42) Caughey, W. S.; Schellenberg, K. A. *J. Org. Chem.* **1966**, *31*, 1978.
(43) Armarego, W. L. F.; Perrin, D. D. *Purification of Laboratory Chemicals*, 4th ed.; Butterworth-Heinemann: Oxford, 1997.
(44) (a) Lin, C.-T.; Böttcher, W.; Chou, M.; Creutz, C.; Sutin, N. *J. Am. Chem. Soc.* **1976**, *98*, 6536. (b) Mercer, E. E.; Buckley, R. R. *Inorg. Chem.* **1965**, *4*, 1692.
(45) Mann, C. K.; Barnes, K. K. *Electrochemical Reactions in Nonaqueous Systems*; Marcel Dekker: New York, 1990.

Scheme 2

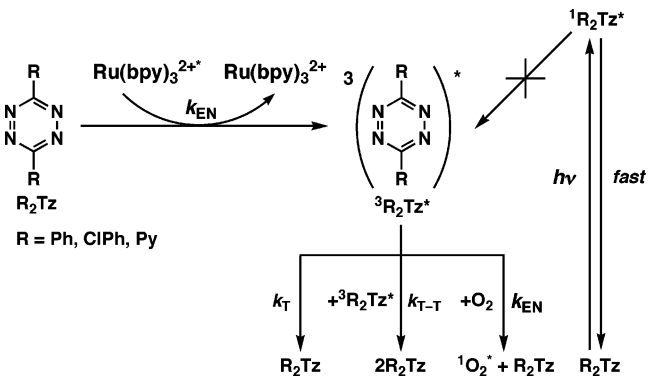

ESR Measurements. Ph_2Tz was dissolved in MeCN (5.6×10^{-3} M in 1.0 mL) and purged with argon for 10 min. 4-*t*-BuBNAH (1.5×10^{-2} M in 1.0 mL) was dissolved in deaerated MeCN. The Ph_2Tz (200 μL) and 4-*t*-BuBNAH (200 μL) solutions were introduced into an ESR cell (1.8 mm i.d.) containing $Ru(bpy)_3^{2+}$ (1.0×10^{-4} M) and mixed by bubbling with Ar gas through a syringe with a long needle. The ESR spectra of the $Ph_2Tz^{\bullet-}$ were recorded on a JEOL JES-RE1XE spectrometer under irradiation of a high-pressure mercury lamp (USH-1005D) focusing at the sample cell in the ESR cavity at 298 K. The magnitude of modulation was chosen to optimize the resolution and signal-to-noise (*S*/*N*) ratio of the observed spectra under nonsaturating microwave power conditions. The *g* value was calibrated using a Mn^{2+} marker.

Results and Discussion

Formation of Triplet Excited States of Tetrazines. No transient absorption spectrum is observed by the laser excitation of 3,6-diphenyl-1,2,4,5-tetrazine (Ph_2Tz) at 355 nm in deaerated acetonitrile (MeCN). When $Ru(bpy)_3^{2+}$ is added to a deaerated MeCN solution of Ph_2Tz, however, the laser excitation at 450 nm affords the formation of a triplet excited state of Ph_2Tz ($^3Ph_2Tz^*$) by energy transfer from $Ru(bpy)_3^{2+*}$ to Ph_2Tz (Scheme 2). The decay at 363 nm due to $Ru(bpy)_3^{2+*}$ ($\epsilon = 2.7 \times 10^4$ M^{-1} cm^{-1}) coincides with the rise in the new absorption band at $\lambda_{max} = 535$ nm ($\epsilon = 3.5 \times 10^3$ M^{-1} cm^{-1}) as shown in Figure 1a.[38,46] When Ph_2Tz is replaced by 3,6-bis(2-chlorophenyl)-1,2,4,5-tetrazine [$(ClPh)_2Tz$] and 3,6-di-2-pyridyl-1,2,4,5-tetrazine (Py_2Tz), the triplet absorption maxima (λ_{max}) are shifted to 530 nm ($\epsilon = 3.0 \times 10^3$ M^{-1} cm^{-1}) and 555 nm ($\epsilon = 4.0 \times 10^3$ M^{-1} cm^{-1}), as shown in Figure 1b and c, respectively. The second-order rate constants (k_{EN}) of energy transfer from $Ru(bpy)_3^{2+*}$ to Ph_2Tz, $(ClPh)_2Tz$, and Py_2Tz in deaerated MeCN are determined as 7.6×10^9 M^{-1} s^{-1}, 1.1×10^{10} M^{-1} s^{-1}, and 8.7×10^9 M^{-1} s^{-1}, respectively (see Supporting Information S1).[38]

In the absence of O_2,[47] $^3R_2Tz^*$ decays through both first-order and second-order processes, which correspond to the unimolecular decay to the ground state and the triplet−triplet (T−T) annihilation, respectively. The time profiles for the decay of $^3R_2Tz^*$ are shown in insets of Figure 1, where the lines are simply best fits which can be fitted well by combined first-order and second-order plots. The initial parts are best fitted by the second-order plot, and the later parts are best fitted by the first-order plots. The first-order decay rate constants (k_T) and

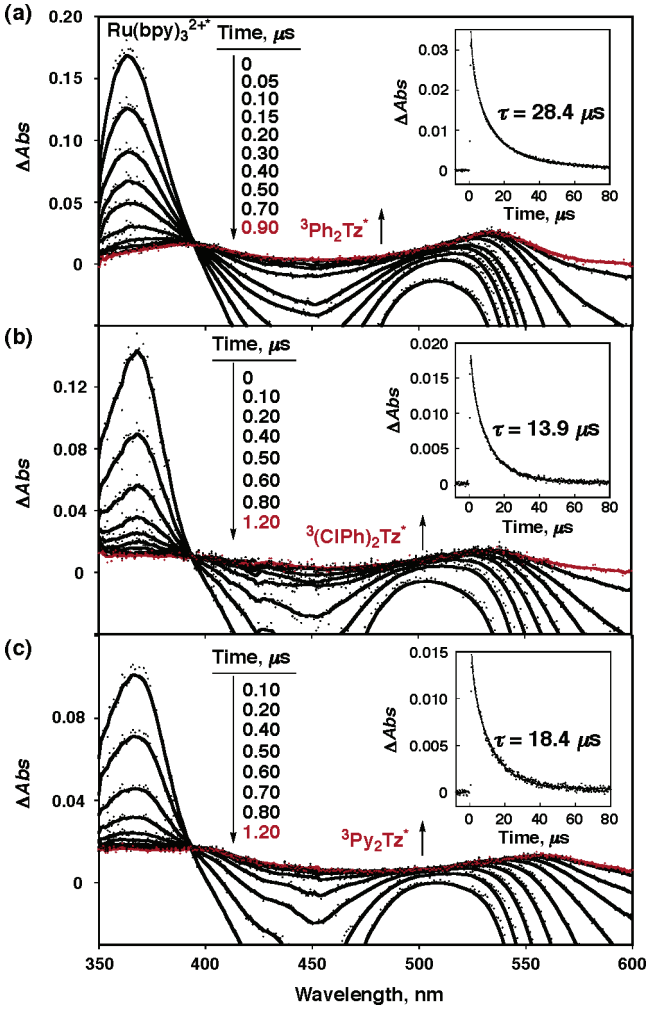

Figure 1. Transient absorption spectra observed by laser flash photolysis of a deaerated MeCN solution of $Ru(bpy)_3^{2+}$ (4.6×10^{-5} M) and (a) Ph_2Tz (9.6×10^{-4} M), (b) $(ClPh)_2Tz$ (9.6×10^{-4} M), and (c) Py_2Tz (9.6×10^{-4} M), at 0−1.2 μs after laser excitation at $\lambda = 450$ nm at 298 K. Insets: Decay time profiles of $^3R_2Tz^*$ at (a) 535 nm, (b) 530 nm, and (c) 555 nm.

the second-order decay rate constants (k_{T-T}) were determined from the slopes of the first-order and second-order plots as k_T: 3.5×10^4 s^{-1} ($^3Ph_2Tz^*$), 7.2×10^4 s^{-1} [$^3(ClPh)_2Tz^*$], 5.4×10^4 s^{-1} ($^3Py_2Tz^*$); k_{T-T}: 2.0×10^{10} M^{-1} s^{-1} ($^3Ph_2Tz^*$, $^3(ClPh)_2Tz^*$, and $^3Py_2Tz^*$); see Supporting Information S5. The lifetimes of $^3R_2Tz^*$ are thereby determined as $\tau = 28.4$ μs ($^3Ph_2Tz^*$), $\tau = 13.9$ μs [$^3(ClPh)_2Tz^*$], and $\tau = 18.4$ μs ($^3Py_2Tz^*$), which are much longer than that of $Ru(bpy)_3^{2+*}$ (0.85 μs).[38−40] The triplet lifetimes are listed in Table S4 together with the reduction potentials (E_{red}) of R_2Tz (see Supporting Information S4). It should be noted that no photochemical decomposition of $^3R_2Tz^*$ was observed in the energy-transfer reactions.[48]

(46) The extinction coefficient (ϵ) of the triplet absorption can be determined from the rise of absorption at 535 nm due to $^3Ph_2Tz^*$ and the decay of absorption at 363 nm due to $Ru(bpy)_3^{2+*}$, because the ϵ value of $Ru(bpy)_3^{2+*}$ has been reported previously; see: Bensasson, R.; Salet, C.; Balzani. V. *J. Am. Chem.* Soc. **1976**, *98*, 3722.

(47) In the presence of O_2, the decay rates of the transient absorption bands observed in Figure 1 increase with increasing concentration of O_2 (see Supporting Information S2a), obeying pseudo-first-order kinetics.[38] The pseudo-first-order rate constant (k_{obs}) increases linearly with concentration of O_2 (see Supporting Information S2b).[38] This indicates that energy transfer from $^3R_2Tz^*$ (R = Ph, ClPh, and Py) to O_2 occurs to produce singlet oxygen ($^1O_2^*$) as shown in Scheme 2. The formation of $^1O_2^*$ ($^1\Delta_g$) was confirmed by observation of the phosphorescence at 1270 nm in an aerated CD_3CN solution of $Ru(bpy)_3^{2+}$ (4.6×10^{-5} M) in the presence of Ph_2Tz (9.6×10^{-4} M); see Supporting Information S3.[38] The second-order rate constants (k_{EN}) of energy transfer from $^3Ph_2Tz^*$, $^3(ClPh)_2Tz^*$, and $^3Py_2Tz^*$ to O_2 are determined from the linear plots of k_{obs} vs concentration of O_2 as 1.1×10^9 M^{-1} s^{-1}, 9.2×10^8 M^{-1} s^{-1}, and 9.2×10^8 M^{-1} s^{-1}, respectively.[38] The k_{EN} values are listed in Table S4 together with the reduction potentials (E_{red}) of R_2Tz (see Supporting Information S4).

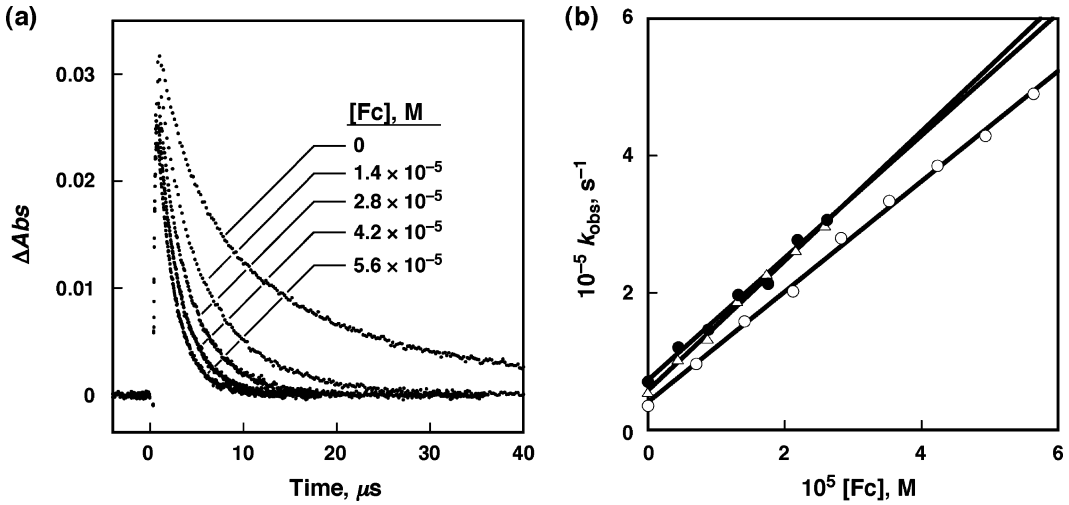

Figure 2. (a) Decay dynamics of the T−T absorption at 535 nm due to $^3Ph_2Tz^*$ observed by laser flash photolysis of Ru(bpy)$_3^{2+}$ (4.6×10^{-5} M) and Ph_2Tz (9.6×10^{-4} M) in the presence of Fc (0 M, 1.4×10^{-5} M, 2.8×10^{-5} M, 4.2×10^{-5} M, and 5.6×10^{-5} M) in deaerated MeCN at 298 K. (b) Plots of k_{obs} of $^3Ph_2Tz^*$ (○), $^3(ClPh)_2Tz^*$ (●), and $^3Py_2Tz^*$ (△) vs [Fc] in deaerated MeCN at 298 K.

Table 1. Oxidation Potentials (E_{ox}) of Electron Donors and Rate Constants (k_{et}) of Electron Transfer from Electron Donors to $^3R_2Tz^*$ in Deaerated MeCN at 298 K

		E_{ox}	k_{et}[a] (M^{-1} s^{-1})		
no.	electron donor	(V vs SCE)	Ph_2Tz	$(ClPh)_2Tz$	Py_2Tz
1	decamethylferrocene	−0.08	1.2×10^{10}	1.7×10^{10}	1.6×10^{10}
2	dimethylferrocene	0.26	9.5×10^{9}	1.2×10^{10}	1.1×10^{10}
3	ferrocene	0.37	7.6×10^{9}	8.9×10^{9}	9.5×10^{9}
4	4-methyl-*N*,*N*-dimethylaniline	0.69	1.5×10^{9}	4.5×10^{9}	4.8×10^{9}
5	*N*,*N*-dimethylaniline	0.78	6.4×10^{8}	1.1×10^{9}	2.6×10^{9}
6	4-bromo-*N*,*N*-dimethylaniline	0.92	1.3×10^{8}	4.2×10^{8}	1.1×10^{9}
7	1,4-dimethoxybenzene	1.34	1.5×10^{5}	4.3×10^{5}	1.5×10^{6}
8	1,3-dimethoxybenzene	1.49	*b*	*b*	8.3×10^{4}

[a] Determined from plots of k_{obs} vs concentrations of electron donors. The experimental error is ±5%. [b] Too small to be determined accurately.

Electron Transfer from Electron Donors to Triplet Excited States of Tetrazines. Since the E_{red} values of R_2Tz are significantly more positive than the value of Ru(bpy)$_3^{2+}$ (see Supporting Information S4), $^3R_2Tz^*$ may act as stronger electron acceptors than Ru(bpy)$_3^{2+*}$. Thus, we have examined the dynamics of photoinduced electron-transfer reactions from a variety of electron donors to $^3R_2Tz^*$.[50]

The triplet excited states ($^3R_2Tz^*$) are quenched efficiently by electron transfer from ferrocene (Fc) to $^3R_2Tz^*$ (eq 2). The

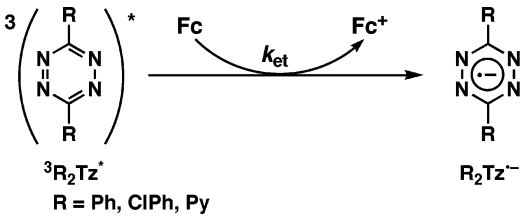

(2)

decay of $^3Ph_2Tz^*$ becomes faster when Fc is added to the Ru(bpy)$_3^{2+}$−Ph_2Tz system as shown in Figure 2a.[38] The decay rate obeys pseudo-first-order kinetics, and the pseudo-first-order rate constants (k_{obs}) increase linearly with increasing concentration of Fc as shown in Figure 2b,[38] where the data of other tetrazines [$(ClPh)_2Tz$ and Py_2Tz] are also included. The second-order rate constants (k_{et}) of electron transfer are determined from the linear plots of k_{obs} vs concentration of Fc, as 7.6×10^9 M^{-1} s^{-1} (Ph_2Tz: open circles),[38] 8.9×10^9 M^{-1} s^{-1} [$(ClPh)_2$-Tz: closed circles], and 9.5×10^9 M^{-1} s^{-1} (Py_2Tz: open triangles). Similarly the k_{et} values of electron transfer from a series of electron donors to $^3R_2Tz^*$ were determined, and the k_{et} values are listed in Table 1 together with the one-electron oxidation potentials of electron donors (E_{ox}).[38] The log k_{et} values increase with decreasing the E_{ox} value to reach a diffusion-limited value (2.0×10^{10} M^{-1} s^{-1}) as shown in Figure 3 (red, blue, and green closed circles for Ph_2Tz,[38] $(ClPh)_2Tz$, and Py_2-Tz, respectively). Such dependence of log k_{et} on E_{ox} is typical for outer-sphere electron-transfer processes.[51] Thus, $^3R_2Tz^*$ is quenched by outer-sphere electron-transfer processes with electron donors.

The dependence of the activation Gibbs energy of photoinduced electron transfer ($\Delta G^{\neq}$) on the Gibbs energy change of electron transfer (ΔG_{et}) has well been established as given by eq 3,[51] where $\Delta G^{\neq}_0$ is the intrinsic barrier that represents the activation Gibbs energy change when the driving force of

$$\Delta G^{\neq} = (\Delta G_{et}/2) + [(\Delta G_{et}/2)^2 + (\Delta G^{\neq}_0)^2]^{1/2} \qquad (3)$$

electron transfer is zero, i.e., $\Delta G^{\neq} = \Delta G^{\neq}_0$ at $\Delta G_{et} = 0$. On

(48) No absorbance change was observed in a deaerated MeCN solution of Ru(bpy)$_3^{2+}$ (4.6×10^{-5} M) in the presence of Ph_2Tz (9.6×10^{-4} M) after 8000 times the laser excitation at 450 nm (laser power: 8.6 mJ).
(49) Kalyanasundaram, K. *Coord. Chem. Rev.* **1982**, *46*, 159.
(50) The triplet energy of $^3R_2Tz^*$ could not be determined from the phosphorescence spectrum that was not observed in frozen media, because $^3R_2Tz^*$ is only formed by intermolecular energy transfer from Ru(bpy)$_3^{2+*}$ to R_2Tz by diffusion.
(51) (a) Rehm D.; Weller, A. *Ber. Bunsen-Ges. Phys. Chem.* **1969**, *73*, 834. (b) Rehm D.; Weller, A. *Isr. J. Chem.* **1970**, *8*, 259.

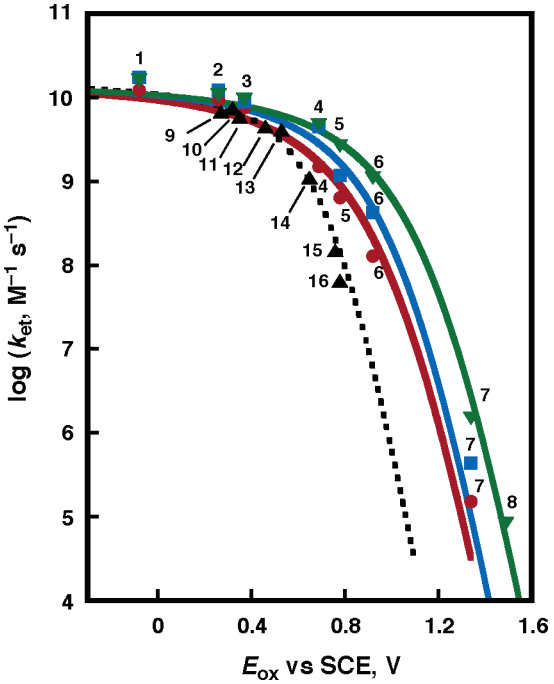

Figure 3. Plots of log k_{et} vs E_{ox} for photoinduced electron transfer from various electron donors to $^3Ph_2Tz^*$ (red closed circles), $^3(ClPh)_2Tz^*$ (blue closed squares), $^3Py_2Tz^*$ (green closed triangles), and $Ru(bpy)_3^{2+*}$ (black closed triangles) in deaerated MeCN at 298 K. Numbers at red closed circles, blue closed squares, and green closed triangles correspond to those in Table 1. Numbers at black closed triangles are taken from ref 36c [9: 4-aminodiphenilamine (E_{ox}: 0.27 V vs SCE; k_{et}: 9.4×10^9 M^{-1} s^{-1}), 10: *N*,*N*,*N*′,*N*′-tetramethylbenzidine (E_{ox}: 0.32 V vs SCE; k_{et}: 1.1×10^{10} M^{-1} s^{-1}), 11: *N*,*N*′-diphenyl-*p*-phenylenediamine (E_{ox}: 0.35 V vs SCE; k_{et}: 8.7×10^9 M^{-1} s^{-1}), 12: benzidine (E_{ox}: 0.46 V vs SCE; k_{et}: 4.5×10^9 M^{-1} s^{-1}), 13: phenothiazine (E_{ox}: 0.53 V vs SCE; k_{et}: 4.1×10^9 M^{-1} s^{-1}), 14: 4-methyl-*N*,*N*-dimethylaniline (E_{ox}: 0.65 V vs SCE; k_{et}: 1.1×10^9 M^{-1} s^{-1}), 15: *N*,*N*-diethylaniline (E_{ox}: 0.76 V vs SCE; k_{et}: 1.5×10^8 M^{-1} s^{-1}), and 16: *N*,*N*-dimethylaniline (E_{ox}: 0.78 V vs SCE; k_{et}: 6.5×10^7 M^{-1} s^{-1})].

the other hand $\Delta G^{\neq}$ values are correlated with the rate constant of electron transfer (k_{et}) as given by eq 4

$$\Delta G^{\neq} = (2.3RT/F)\log[Z(k_{et}^{-1} - k_{diff}^{-1})] \qquad (4)$$

where Z is the collision frequency that is taken as 1×10^{11} M^{-1} s^{-1}, F is the Faraday constant, and k_{diff} is the diffusion rate constant in MeCN (2.0×10^{10} M^{-1} s^{-1}).[51] The ΔG_{et} values are obtained from the one-electron oxidation potentials of electron donors (E_{ox}) and the one-electron reduction potentials of $^3R_2Tz^*$ (E_{red}*) by eq 5.

$$\Delta G_{et} = F(E_{ox} - E_{red}^*) \qquad (5)$$

The plots of Figure 3 are fitted using eqs 3−5 with two unknown parameters, i.e., E_{red}* and $\Delta G^{\neq}_0$, as shown by the solid lines, which agrees with the experimental results. The E_{red}* and $\Delta G^{\neq}_0$ values were determined as 1.09 ± 0.04 V vs SCE ($^3Ph_2Tz^*$);[38] 1.11 ± 0.05 V vs SCE: $^3(ClPh)_2Tz^*$; 1.25 ± 0.04 V vs SCE ($^3Py_2Tz^*$)] and [5.24 ± 0.59 kcal mol^{-1} ($^3Ph_2Tz^*$);[38] 4.70 ± 0.22 kcal mol^{-1}: $^3(ClPh)_2Tz^*$; 5.10 ± 0.45 kcal mol^{-1} ($^3Py_2Tz^*$), respectively from the best fit lines in Figure 3. The plot of log k_{et} vs E_{ox} for electron transfer from $Ru(bpy)_3^{2+*}$ to a similar series of electron donors is also shown in Figure 3 (black closed triangles) for comparison.[36c] The plot of $Ru(bpy)_3^{2+*}$ is significantly shifted to a negative direction (−0.48 eV) in accordance with the difference in the E_{red}* values between $Ru(bpy)_3^{2+*}$ (0.77 V vs SCE)[40] and $^3Py_2Tz^*$ (1.25 ± 0.04 V vs SCE). The triplet excited-state energies of $^3R_2Tz^*$ are determined by subtracting the E_{red} value of R_2Tz [−0.91 V vs SCE (Ph_2Tz); −0.78 V vs SCE ($ClPh)_2Tz$; −0.85 V vs SCE (Py_2Tz)] from the E_{red}* values, as 2.00 ± 0.04 eV ($^3Ph_2Tz^*$), 1.89 ± 0.05 eV [$^3(ClPh)_2Tz^*$], and 2.10 ± 0.04 eV ($^3Py_2Tz^*$). The E_{red} values were determined by the cyclic voltammetry measurements (see Supporting Information S6). The E_{red}* and $\Delta G^{\neq}_0$ values are listed in Table S4 (see Supporting Information S4).

One-Step Hydrogen Transfer vs Rate-Limiting Electron Transfer from $AcrH_2$ to Triplet Excited States of Tetrazines. 10-Methyl-9,10-dihydroacridine ($AcrH_2$) has frequently been used as an NADH analogue, because $AcrH_2$ acts as a hydride donor like NADH.[19,21a,22,29] The C(9)−H bond of $AcrH_2$ is relatively weak, and the hydrogen is readily abstracted by radical species.[30a] We examined the dynamics of hydrogen transfer from $AcrH_2$ to $^3Ph_2Tz^*$. The laser flash photolysis of a deaerated MeCN solution of $Ru(bpy)_3^{2+}$ (4.6×10^{-5} M) at 450 nm in the presence of Ph_2Tz (9.6×10^{-5} M) and $AcrH_2$

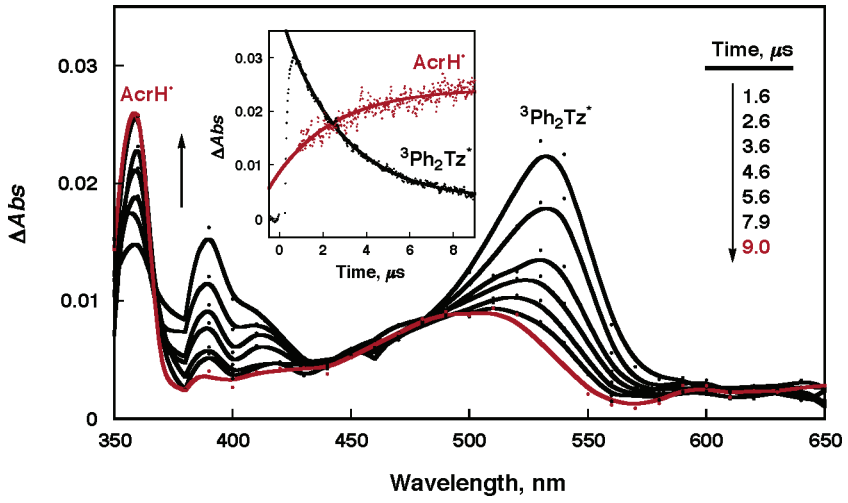

Figure 4. Transient absorption spectra observed by laser flash photolysis of a deaerated MeCN solution of $Ru(bpy)_3^{2+}$ (4.6×10^{-5} M) in the presence of $AcrH_2$ (1.1×10^{-4} M) and Ph_2Tz (9.6×10^{-4} M) at 1.6−9.0 μs after laser excitation at λ = 450 nm at 298 K. Inset: Time profiles of the decay of absorbance at 535 nm due to $^3Ph_2Tz^*$ (black closed circles) and the rise of absorbance at 360 nm due to $AcrH^•$ (red closed circles).

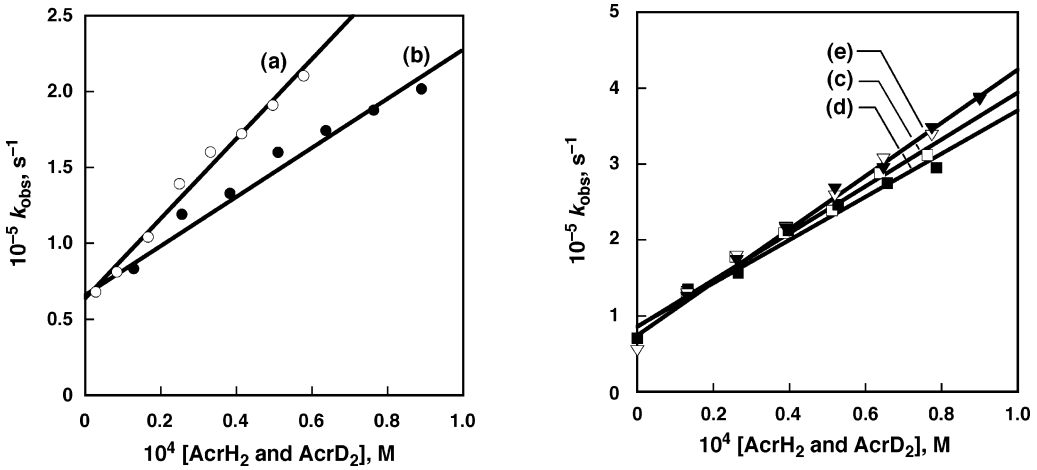

Figure 5. Plots of k_{obs} vs [$AcrH_2$] and [$AcrD_2$] for the reactions of $^3Ph_2Tz^*$ with (a) $AcrH_2$ (○) and (b) $AcrD_2$ (●), the reactions of $^3(ClPh)_2Tz^*$ with (c) $AcrH_2$ (□) and (d) $AcrD_2$ (■), and (e) the reactions of $^3Py_2Tz^*$ with $AcrH_2$ (▽) and $AcrD_2$ (▼) in deaerated MeCN at 298 K.

Table 2. pK_a Values of Radical Cations of NADH Analogues, Oxidation Potentials (E_{ox}) of NADH Analogues, Reduction Potentials (E_{red}*) of $^3R_2Tz^*$, Gibbs Energy Change (ΔG_{et}) of Electron Transfer from NADH Analogues to $^3R_2Tz^*$ and Ru(bpy)$_3^{2+*}$, Rate Constants of Quenching of $^3R_2Tz^*$ and Ru(bpy)$_3^{2+*}$ by NADH Analogues (k_H) and NADH-4,4′-d_2 Analogues (k_D), and the Primary Deuterium Kinetic Isotope Effects (k_H/k_D) in Deaerated MeCN at 298 K

no.	tetrazine and Ru(bpy)$_3^{2+}$	NADH analogue	pK_a[a]	E_{ox} (V vs SCE)	E_{red}* (V vs SCE)	ΔG_{et}[e] (eV)	k_H (M^{-1} s^{-1})	k_D (M^{-1} s^{-1})	k_H/k_D
17	Ph_2Tz	$AcrH_2$ ($AcrD_2$)	2.0	0.81	1.09 ± 0.04[c]	−0.28 ± 0.04	(2.7 ± 0.1) × 10^9 [f]	(1.5 ± 0.1) × 10^9 [f]	1.80 ± 0.20
18	$(ClPh)_2Tz$	$AcrH_2$ ($AcrD_2$)	2.0	0.81	1.11 ± 0.05[c]	−0.30 ± 0.05	(3.1 ± 0.1) × 10^9 [f]	(2.8 ± 0.1) × 10^9 [f]	1.11 ± 0.08
19	Py_2Tz	$AcrH_2$ ($AcrD_2$)	2.0	0.81	1.25 ± 0.04[c]	−0.44 ± 0.04	(3.4 ± 0.1) × 10^9 [f]	(3.4 ± 0.1) × 10^9 [f]	1.00 ± 0.06
20	Ru(bpy)$_3^{2+}$	$AcrH_2$ ($AcrD_2$)	2.0	0.81	0.77[d]	+0.04	(2.2 ± 0.1) × 10^8 [g]	(2.2 ± 0.1) × 10^8 [g]	1.00 ± 0.05
21	$(ClPh)_2Tz$	$AcrHPr^i$	*b*	0.84	1.11 ± 0.05[c]	−0.27 ± 0.05	1.0 × 10^9 [f,h]		
22	Ru(bpy)$_3^{2+}$	$AcrHPr^i$	*b*	0.84	0.77[d]	+0.07	(6.9 ± 0.2) × 10^7 [g]		
23	Ph_2Tz	BNAH (BNAH-4,4′-d_2)	3.6	0.57	1.09 ± 0.04[e]	−0.52 ± 0.04	(3.6 ± 0.1) × 10^9 [f]	(3.6 ± 0.1) × 10^9 [f]	1.00 ± 0.06
24	$(ClPh)_2Tz$	BNAH (BNAH-4,4′-d_2)	3.6	0.57	1.11 ± 0.05[c]	−0.54 ± 0.05	(4.4 ± 0.2) × 10^9 [f]	(4.4 ± 0.2) × 10^9 [f]	1.00 ± 0.10
25	Py_2Tz	BNAH (BNAH-4,4′-d_2)	3.6	0.57	1.25 ± 0.04[c]	−0.68 ± 0.04	(4.6 ± 0.1) × 10^9 [f]	(4.6 ± 0.1) × 10^9 [f]	1.00 ± 0.04
26	Ru(bpy)$_3$	BNAH (BNAH-4,4′-d_2)	3.6	0.57	0.77[d]	−0.20	1.0 × 10^9 [g,h]	1.0 × 10^9 [g]	1.00 ± 0.08

[a] Taken from ref 19. [b] pK_a value of $AcrHPr^{i\bullet+}$ may be slightly larger than the pK_a value of $AcrH_2^{\bullet+}$.[22] [c] Determined from rates of outer-sphere electron transfer from electron donors to $^3R_2Tz^*$. [d] Taken from ref 40. [e] Obtained by subtracting the E_{red}* values from the E_{ox} values. [f] Determined from plots of k_{obs} vs concentrations of NADH analogues and NADH-4,4′-d_2 analogues. [g] Determined from the Stern−Volmer plots for the emission quenching of Ru(bpy)$_3^{2+*}$. [h] The experimental error is ±4%.

(1.1×10^{-4} M) with 450 nm laser light results in the appearance of new absorption bands due to $AcrH^\bullet$ (λ_{max} = 360 and 520 nm)[52] with a concomitant decrease in the absorption band due to $^3Ph_2Tz^*$ (λ_{max} = 535 nm) as shown in the red line in Figure 4, whereas no absorption band due to the $AcrH_2^{\bullet+}$ (λ_{max} = 640 nm)[23a] is observed.[53,54]

Whether hydrogen transfer from $AcrH_2$ to $^3Ph_2Tz^*$ occurs via a one-step hydrogen transfer or a rate-determining electron transfer followed by fast proton transfer can be clarified by examining the deuterium kinetic isotope effects. The one-step hydrogen transfer would afford a significant deuterium kinetic isotope effect, whereas the rate-determining electron transfer followed by fast proton transfer would exhibit no deuterium kinetic isotope effect. In fact, no deuterium kinetic isotope effect is observed in the emission quenching of Ru(bpy)$_3^{2+*}$ by $AcrH_2$, where electron transfer from $AcrH_2$ to Ru(bpy)$_3^{2+*}$ occurs as shown in Scheme 3a (see Supporting Information S7). In

Scheme 3

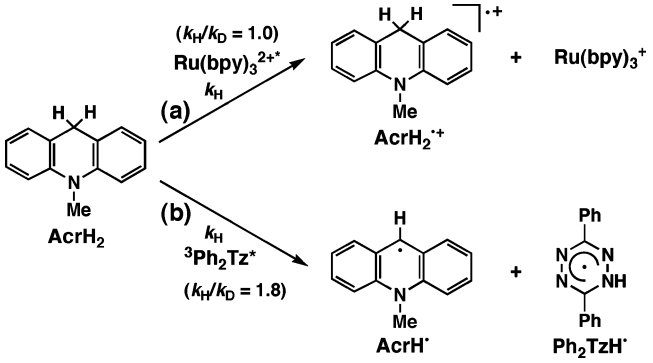

contrast to the case of Ru(bpy)$_3^{2+*}$, the hydrogen transfer to $^3Ph_2Tz^*$ exhibits a significant primary deuterium kinetic isotope effect (k_H/k_D = 1.80 ± 0.20) [Figure 5a and b]. In such a case, the hydrogen transfer from $AcrH_2$ to $^3Ph_2Tz^*$ occurs via a one-step process as shown in Scheme 3b, which should be faster than electron transfer from $AcrH_2$ to $^3Ph_2Tz^*$. The observed rate constant of hydrogen transfer from $AcrH_2$ to $^3Ph_2Tz^*$ is indeed larger than the expected value of electron transfer from $AcrH_2$ to $^3Ph_2Tz^*$ (vide infra).

The kinetic data of hydrogen transfer from $AcrH_2$ to $^3Ph_2Tz^*$ and Ru(bpy)$_3^{2+*}$ are listed in Table 2 together with the one-

(52) (a) Ohkubo, K.; Suga, K.; Morikawa, K.; Fukuzumi, S. *J. Am. Chem. Soc.* **2003**, *125*, 12850. (b) Fukuzumi, S.; Ohkubo, K.; Suenobu, T.; Kato, K.; Fujitsuka, M.; Ito, O. *J. Am. Chem. Soc.* **2001**, *123*, 8459.

(53) The $AcrH^\bullet$ is not formed by the hydrogen transfer from $AcrH_2$ to Ru(bpy)$_3^{2+*}$ but to $^3Ph_2Tz^*$, since Ru(bpy)$_3^{2+*}$ is completely quenched by Ph_2Tz under the present experimental conditions.

(54) The transient absorption spectrum of the other product of hydrogen transfer, $Ph_2TzH^\bullet$, may be negligibly small in the region of 350−650 nm, judging from the weak absorption band of the one-electron reduced product of Ph_2Tz ($Ph_2Tz^{\bullet-}$); see Supporting Information S8.

electron oxidation potentials of NADH analogues and pK_a values of the radical cations.

Plots of log k_{et} of electron transfer from various electron donors to $^3R_2Tz^*$ vs the Gibbs energy change of electron transfer (ΔG_{et}) are shown in Figure 6, where the solid lines are drawn based on eqs 3−5 for the electron-transfer reactions. The observed rate constant of hydrogen transfer from $AcrH_2$ to $^3Ph_2Tz^*$ [$k_H = (2.7 \pm 0.1) \times 10^9$ M^{-1} s^{-1} in Table 2] is also included in Figure 6a (no. 17), and this is significantly larger than the expected value from the plot of log k_{et} vs ΔG_{et}. In contrast, the observed quenching-rate constant of $Ru(bpy)_3^{2+*}$ by $AcrH_2$ [$k_H = (2.2 \pm 0.1) \times 10^8$ M^{-1} s^{-1} in Table 2] agrees well with the correlation of log k_{et} vs ΔG_{et} for the electron-transfer reactions (no. 20 in Figure 6d), because the emission of $Ru(bpy)_3^{2+*}$ is quenched by the electron-transfer reaction from $AcrH_2$ (Scheme 3a).

When $^3Ph_2Tz^*$ ($E_{red}^* = 1.09 \pm 0.04$ V vs SCE) is replaced by a tetrazine derivative which has a slightly higher reduction potential of $^3(ClPh)_2Tz^*$ ($E_{red}^* = 1.11 \pm 0.05$ V vs SCE), $AcrH^\bullet$ is also generated by hydrogen transfer from $AcrH_2$ to $^3(ClPh)_2Tz^*$ (see Supporting Information S9). In contrast to the case of $^3Ph_2Tz^*$, a small primary kinetic isotope effect ($k_H/k_D = 1.11 \pm 0.08$) is observed (Figure 5c and d). The observed rate constant of hydrogen transfer from $AcrH_2$ to $^3(ClPh)_2Tz^*$ [$k_H = (3.1 \pm 0.1) \times 10^9$ M^{-1} s^{-1} in Table 2] is roughly the same as the expected value from the correlation for the electron-transfer reactions (no. 18 in Figure 6b). This indicates a one-step hydrogen-transfer process and the rate-determining electron transfer followed by rapid proton transfer occur competitively in hydrogen transfer from $AcrH_2$ to $^3(ClPh)_2Tz^*$ as shown in Scheme 4. The hydrogen transfer from $AcrH_2$ to $^3(ClPh)_2Tz^*$ (no. 18 in Figure 6b) may be a mechanistic borderline where the one-step hydrogen-transfer pathway is changed to the rate-determining electron transfer followed by rapid proton-transfer pathway in hydrogen transfer from $AcrH_2$ to a series of a tetrazine derivatives. The Gibbs energy change of electron transfer from $AcrH_2$ ($E_{ox} = 0.81$ V vs SCE) to $^3(ClPh)_2Tz^*$ ($E_{red}^* = 1.11 \pm 0.05$ V vs SCE) [$\Delta G_{et} = -0.30$ eV] is shown in Figure 6a−c dashed line to emphasis the mechanistic borderline. When ΔG_{et} becomes smaller than −0.30 eV, the reaction mechanism would be changed to the rate-determining electron transfer followed by rapid proton transfer. In fact, no deuterium kinetic isotope effect is observed (Figure 5e), when $^3(ClPh)_2Tz^*$ ($E_{red}^* = 1.11 \pm 0.05$ V vs SCE) is replaced by a tetrazine derivative, $^3Py_2Tz^*$ ($E_{red}^* = 1.25 \pm 0.04$ V vs SCE), which has a stronger oxidizing ability than $^3(ClPh)_2Tz^*$. In this case, the observed rate constant of hydrogen transfer from $AcrH_2$ to $^3Py_2Tz^*$ [$k_H = (3.4 \pm 0.1) \times 10^9$ M^{-1} s^{-1} in Table 2] agrees with the expected value from the plot of log k_{et} vs ΔG_{et} (no. 19 in Figure 6c).

The basicity of the nitrogen sites of tetrazine derivatives is also an essential factor to determine the reaction mechanism. The basicity of $R_2Tz^{\bullet-}$ of the nitrogen sites will decrease in the order $Ph_2Tz^{\bullet-}$ > $Py_2Tz^{\bullet-}$ > $(ClPh)_2Tz^{\bullet-}$ judging from E_{red} values of tetrazine derivatives [−0.91 V vs SCE (Ph_2Tz); −0.85 V vs SCE (Py_2Tz); −0.78 V vs SCE ($ClPh)_2Tz$]. The strong basic sites of $R_2Tz^{\bullet-}$ will afford very fast proton transfer. In such a case, the proton transfer may be fast enough to couple with electron transfer, which is the net hydrogen transfer. Hydrogen transfer from $AcrH_2$ to $^3Ph_2Tz^*$ is only a single

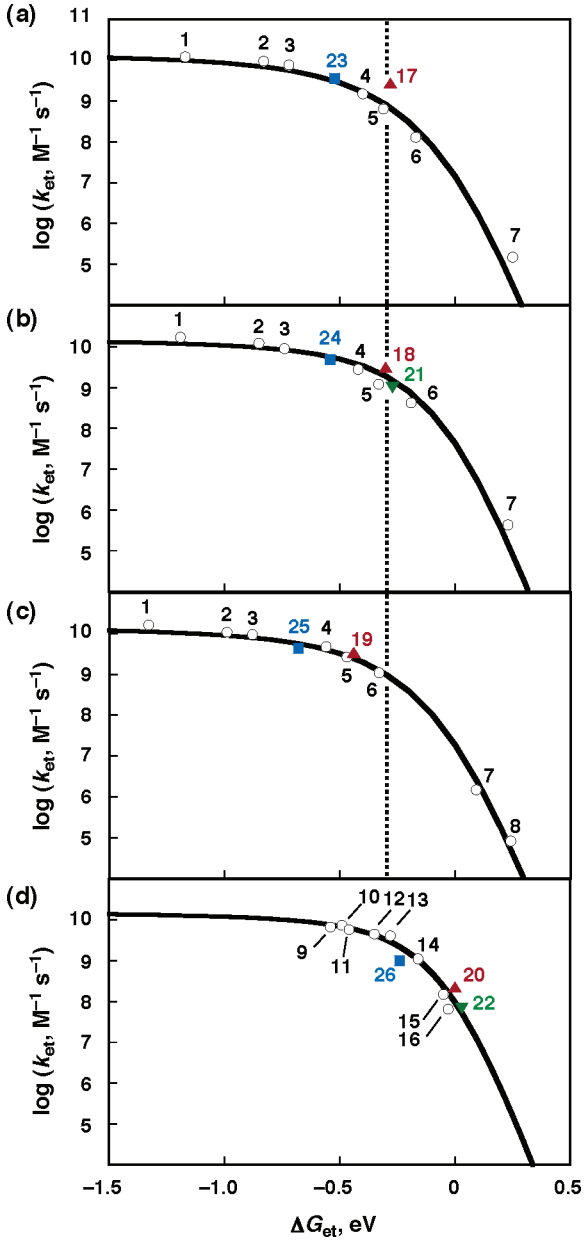

Figure 6. (a) Plots of log k_{et} vs ΔG_{et} for photoinduced electron transfer from various electron donors to $^3Ph_2Tz^*$ (open circles), including plots of log k_H vs ΔG_{et} for quenching of $^3Ph_2Tz^*$ by $AcrH_2$ (red closed triangles) and BNAH (blue closed squares) in deaerated MeCN at 298 K. (b) Plots of log k_{et} vs ΔG_{et} for photoinduced electron transfer from various electron donors to $^3(ClPh)_2Tz^*$ (open circles), including plots of log k_H vs ΔG_{et} for quenching of $^3(ClPh)_2Tz^*$ by $AcrH_2$ (red closed triangles), BNAH (blue closed squares), and $AcrHPr^i$ (green closed triangles) in deaerated MeCN at 298 K. (c) Plots of log k_{et} vs ΔG_{et} for photoinduced electron transfer from various electron donors to $^3Py_2Tz^*$ (open circles), including plots of log k_H vs ΔG_{et} for quenching of $^3Py_2Tz^*$ by $AcrH_2$ (red closed triangles) and BNAH (blue closed squares) in deaerated MeCN at 298 K. (d) Plots of log k_{et} vs ΔG_{et} for photoinduced electron transfer from various electron donors to $Ru(bpy)_3^{2+*}$ (open circles), including plots of log k_H vs ΔG_{et} for emission quenching of $Ru(bpy)_3^{2+}$ by $AcrH_2$ (red closed triangles), BNAH (blue closed squares), and $AcrHPr^i$ (green closed triangles) in deaerated MeCN at 298 K. Numbers at open circles (numbers 1−8) correspond to those in Table 1. Numbers at open circles (numbers 9−16) are taken from ref 36c [9: 4-aminodiphenilamine, 10: *N*,*N*,*N*′,*N*′-tetramethylbenzidine, 11: *N*,*N*′-diphenyl-*p*-phenylenediamine, 12: benzidine, 13: phenothiazine, 14: 4-methyl-*N*,*N*-dimethylaniline, 15: *N*,*N*-diethylaniline, and 16: *N*,*N*-dimethylaniline]. Numbers at closed red and green triangles and blue closed squares correspond to those in Table 2.

Scheme 4

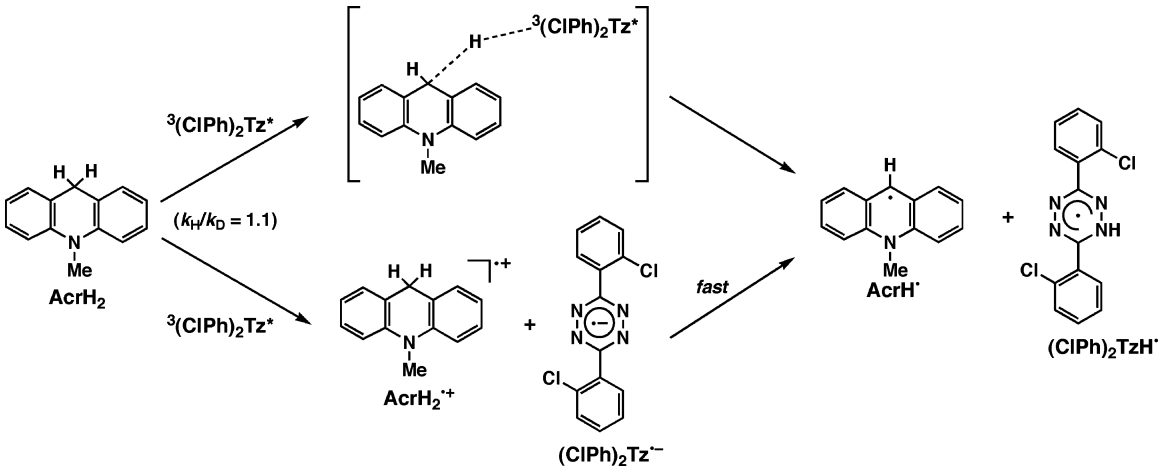

distinct example of the one-step mechanism, because the ^{3}Ph$_2$Tz* is the weakest electron acceptor and base in R$_2$Tz. Thus, the mechanism of hydrogen transfer is changed from the one-step hydrogen transfer to the rate-determining electron transfer followed by rapid proton transfer, with increasing the E_{red}* value and decreasing the basicity of the nitrogen sites of ^{3}R$_2$Tz*.

The AcrH$^\bullet$ formed by hydrogen transfer from AcrH$_2$ to ^{3}R$_2$Tz* decays obeying second-order kinetics, which corresponds to back hydrogen-transfer processes from Ph$_2$TzH$^\bullet$ and (ClPh)$_2$TzH$^\bullet$ to AcrH$^\bullet$ (see Supporting Information S10). There is no deuterium kinetic isotope effect in the back hydrogen-transfer processes of AcrH$^\bullet$, since the rate constants are close to a diffusion-limited value.[55]

Electron Transfer from AcrHPr^i to Ru(bpy)$_3^{2+*}$ and Sequential Electron and Proton Transfer from AcrHPr^i to ^{3}(ClPh)$_2$Tz*. The replacement of the C(9)−H hydrogen of AcrH$_2$ by isopropyl group (AcrHPr^i) is known to retard the deprotonation from AcrHPr$^{i\bullet+}$ because of the steric hindrance

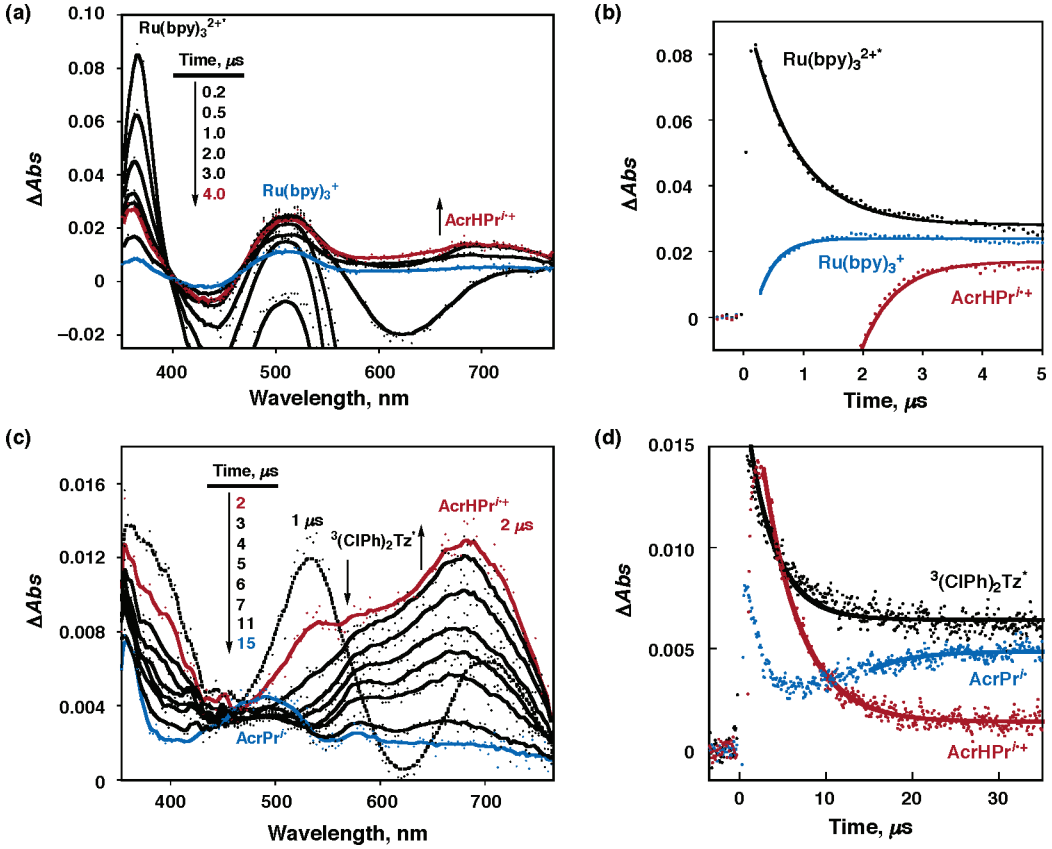

Figure 7. (a) Transient absorption spectra observed by laser flash photolysis of a deaerated MeCN solution of Ru(bpy)$_3^{2+}$ (4.6×10^{-5} M) in the presence of AcrHPr^i (1.0×10^{-2} M) at 0.2−4.0 μs after laser excitation at $\lambda = 450$ nm at 298 K. (b) Time profiles of the decay of absorbance at 363 nm due to Ru(bpy)$_3^{2+*}$ (black closed circles), the rise of absorbance at 510 nm due to Ru(bpy)$_3^+$ (blue closed circles), and the rise of absorbance at 680 nm due to AcrHPr$^{i\bullet+}$ (red closed circles). (c) Transient absorption spectra observed by laser flash photolysis of a deaerated MeCN solution of Ru(bpy)$_3^{2+}$ (4.6×10^{-5} M) in the presence of AcrHPr^i (8.8×10^{-4} M) and (ClPh)$_2$Tz (9.6×10^{-4} M) at 1−15 μs after laser excitation at $\lambda = 450$ nm at 298 K. (d) Time profiles of the decay of absorbance at 530 nm due to ^{3}(ClPh)$_2$Tz* (black closed circles), the decay of absorbance at 680 nm due to AcrHPr$^{i\bullet+}$ (red closed circles), and the rise of absorbance at 510 nm due to AcrPr$^{i\bullet}$ (blue closed circles).

Scheme 5

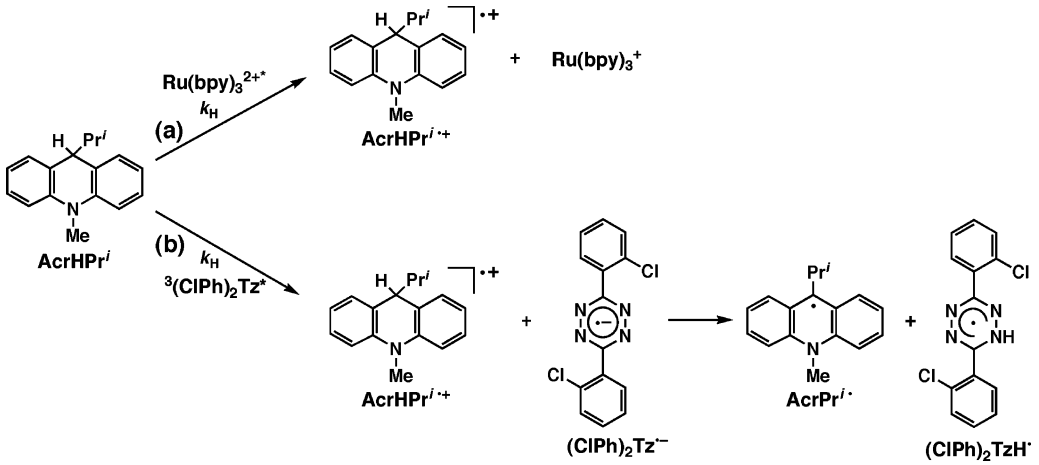

of the Pr^i group.[23a] When $AcrH_2$ is replaced by AcrHPr^i in the hydrogen-transfer reaction with $Ru(bpy)_3^{2+*}$, the absorption band due to AcrHPr$^{i\bullet+}$ (λ_{max} = 680 nm)[23a] appears together with the absorption band due to $Ru(bpy)_3^{+}$ (λ_{max} = 510 nm; $\epsilon = 1.4 \times 10^4$ M^{-1} cm^{-1})[49] at 4 μs after the laser excitation of $Ru(bpy)_3^{2+}$ at 450 nm in the presence of AcrHPr^i in deaerated MeCN, as shown in Figure 7a, where the bleaching (at 450 nm) due to the $Ru(bpy)_3^{2+}$ is observed (time profiles of the decay of absorbance due to $Ru(bpy)_3^{2+*}$ and the rise of absorbance due to $Ru(bpy)_3^{+}$ are shown in Figure 7b). Thus, electron transfer from AcrHPr^i to $Ru(bpy)_3^{2+*}$ occurs without the subsequent proton transfer as shown in Scheme 5a. The second-order rate constant of electron transfer from AcrHPr^i to $Ru(bpy)_3^{2+*}$, determined from emission quenching of $Ru(bpy)_3^{2+*}$ by AcrHPr^i [$k_H = (6.9 \pm 0.2) \times 10^7$ M^{-1} s^{-1} in Table 2], also agrees with the correlation of log k_{et} vs ΔG_{et} (no. 22 in Figure 6d).[56]

The laser flash excitation (450 nm) of a deaerated MeCN solution of $Ru(bpy)_3^{2+}$ (4.6×10^{-5} M) and AcrHPr^i (8.8×10^{-4} M) in the presence of $(ClPh)_2Tz$ (9.6×10^{-4} M) also results in formation of AcrHPr$^{i\bullet+}$ (λ_{max} = 680 nm)[23a] as shown in Figure 7c (red solid line). The time profiles of the transient absorption at 530 nm due to $^3(ClPh)_2Tz^*$, at 680 nm due to AcrHPr$^{i\bullet+}$, and at 510 nm due to AcrPr$^{i\bullet}$ are shown in Figure 7d (black, red, and blue closed circles, respectively). The absorption at 530 nm due to $^3(ClPh)_2Tz^*$ decays immediately within 2 μs after laser excitation, accompanied by the rise in absorption at 680 nm due to AcrHPr$^{i\bullet+}$. The decay of absorbance at 680 nm due to AcrHPr$^{i\bullet+}$ (red closed circles in Figure 7d) coincides with the rise in absorbance at 510 nm due to AcrPr$^{i\bullet}$ (blue closed circles in Figure 7d). This indicates that electron transfer from AcrHPr^i to $^3(ClPh)_2Tz^*$ occurs rapidly to produce AcrHPr$^{i\bullet+}$ and $(ClPh)_2Tz^{\bullet-}$ within 2 μs, followed by the slower proton transfer from AcrHPr$^{i\bullet+}$ to $(ClPh)_2Tz^{\bullet-}$ to produce AcrPr$^{i\bullet}$ (blue solid line in Figure 7c) as shown in Scheme 5b.[55] The second-order rate constant of electron transfer from AcrHPr^i to $^3(ClPh)_2Tz^*$, determined from the linear plot of the observed triplet decay rate constant (k_{obs}) vs concentration of AcrHPr^i (1.0×10^9 M^{-1} s^{-1} in Table 2), agrees with the correlation of log k_{et} vs ΔG_{et} (no. 21 in Figure 6b).

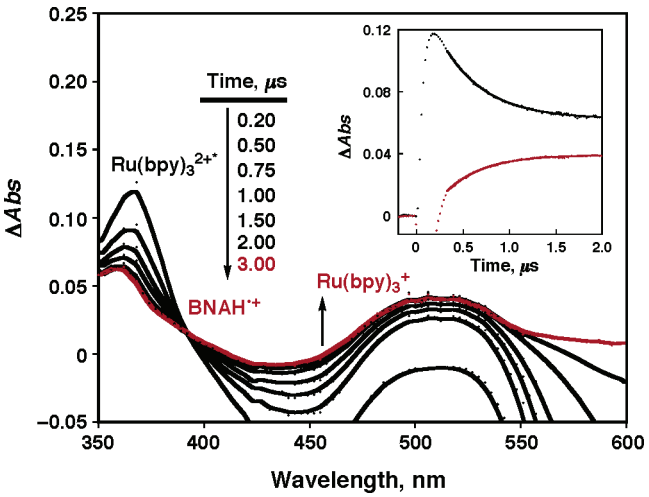

Figure 8. Transient absorption spectra observed by laser flash photolysis of a deaerated MeCN solution of $Ru(bpy)_3^{2+}$ (4.6×10^{-5} M) in the presence of BNAH (1.1×10^{-3} M) at 0.2−3.0 μs after laser excitation at λ = 450 nm at 298 K. Inset: Time profiles of the decay of absorbance at 363 nm due to $Ru(bpy)_3^{2+*}$ (black closed circles) and the rise of absorbance at 510 nm due to $Ru(bpy)_3^{+}$ (red closed circles).

Electron Transfer from BNAH to $Ru(bpy)_3^{2+*}$ and Sequential Electron and Proton Transfer from BNAH to Triplet Excited States of Tetrazines. 1-Benzyl-1,4-dihydronicotinamide (BNAH) is the most commonly used NADH analogue. The dynamics of the reaction of BNAH with $Ru(bpy)_3^{2+*}$ was also examined. At 3 μs after the laser excitation of a deaerated MeCN solution of BNAH (1.1×10^{-3} M) and $Ru(bpy)_3^{2+}$ (4.6×10^{-5} M) at 450 nm, the absorption band at 360 nm due to the BNAH$^{\bullet+}$ is observed together with the absorption band due to $Ru(bpy)_3^{+}$ (λ_{max} = 510 nm),[49] as shown in Figure 8.[20] This indicates that electron transfer from BNAH to $Ru(bpy)_3^{2+*}$ produces BNAH$^{\bullet+}$ and $Ru(bpy)_3^{+}$ as shown in Scheme 6a.[55,57] The subsequent proton transfer from BNAH$^{\bullet+}$ to $Ru(bpy)_3^{+}$ is not observed, because the pK_a value of BNAH$^{\bullet+}$ (3.6 in Table 2) is significantly larger than that of $AcrH_2^{\bullet+}$ (2.0 in Table 2). The second-order rate constant of electron transfer from BNAH to $Ru(bpy)_3^{2+*}$, determined from emission quenching of $Ru(bpy)_3^{2+*}$ by BNAH ($k_H = 1.0 \times 10^9$ M^{-1} s^{-1} in Table 2), agrees with the correlation of log k_{et} vs ΔG_{et} (no. 26 in Figure 6d).

(55) The kinetic data for the back hydrogen-transfer and back electron-transfer processes are given in Supporting Information S11.
(56) The k_H value is virtually the same as that determined from the linear plot of the observed rate constant (k_{obs}) vs concentration of AcrHPr^i for the decay of absorbance at 363 nm due to $Ru(bpy)^{2+*}$ in the presence of AcrHPr^i in deaerated MeCN at 298 K.
(57) The decay rate of BNAH$^{\bullet+}$ obeys second-order kinetics, which corresponds to back electron transfer from $Ru(bpy)_3^{+}$ to BNAH$^{\bullet+}$; see Supporting Information S12.

Scheme 6

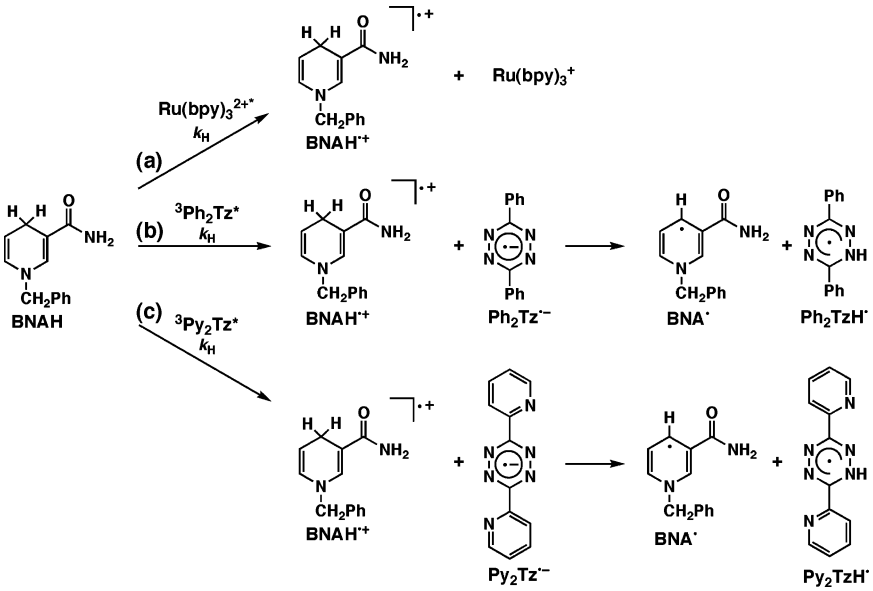

The dynamics of hydrogen transfer from BNAH to ^{3}Ph$_2$Tz* was also examined by laser flash photolysis measurements. The transient absorption band at 380 nm due to BNAH$^{\bullet+}$ appears, overlapping with transient bleaching (at 350−400 nm) due to Ph$_2$Tz at 5 μs after laser excitation of a deaerated MeCN solution of Ru(bpy)$_3$ (4.6×10^{-5} M) and BNAH (1.6×10^{-4} M) in the presence of Ph$_2$Tz (9.6×10^{-4} M) as shown in Figure 9. This indicates that electron transfer from BNAH to ^{3}Ph$_2$Tz* occurs to produce BNAH$^{\bullet+}$ and Ph$_2$Tz$^{\bullet-}$.

The time course of the rise and decay of the transient absorption at 380 and 535 nm is shown in Figure 9 inset (closed red and black closed circles, respectively). The absorption at 535 nm due to ^{3}Ph$_2$Tz* disappears immediately upon the laser excitation within 5 μs (black closed circles) via electron transfer to produce BNAH$^{\bullet+}$ which has an absorption band at 380 nm.

Then, the rise of absorbance at 380 nm is observed due to formation of BNA$^\bullet$ by proton transfer from BNAH$^{\bullet+}$ to Ph$_2$Tz$^{\bullet-}$.[55,58] Thus, electron transfer from BNAH to ^{3}Ph$_2$Tz* occurs to produce BNAH$^{\bullet+}$ and Ph$_2$Tz$^{\bullet-}$, followed by proton transfer from BNAH$^{\bullet+}$ to Ph$_2$Tz$^{\bullet-}$ to yield BNA$^\bullet$ as shown in Scheme 6b.[59] Virtually the same results were obtained in the case of ^{3}Py$_2$Tz* (Scheme 6c; see Supporting Information S14). The quenching rate constant (k_H) of ^{3}Ph$_2$Tz*, ^{3}(ClPh)$_2$Tz*, and ^{3}Py$_2$Tz* by BNAH were determined as $(3.6 \pm 0.1) \times 10^9$ M^{-1} s^{-1}, $(4.4 \pm 0.2) \times 10^9$ M^{-1} s^{-1}, and $(4.6 \pm 0.1) \times 10^9$ M^{-1} s^{-1}, from the linear plots of the observed triplet decay rate constant (k_{obs}) vs concentration of BNAH, respectively (Figure 10).[60]

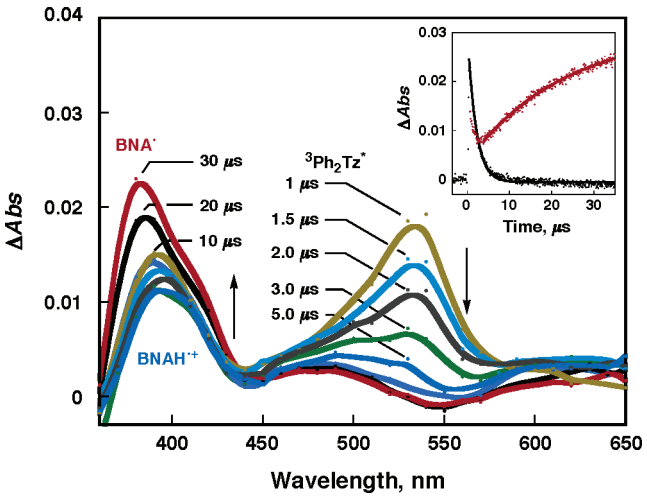

Figure 9. Transient absorption spectra observed by laser flash photolysis of a deaerated MeCN solution of Ru(bpy)$_3^{2+}$ (4.6×10^{-5} M) in the presence of BNAH (1.6×10^{-4} M) and Ph$_2$Tz (9.6×10^{-4} M) at 1.0−30 μs after laser excitation at $\lambda = 450$ nm at 298 K. Inset: Time profiles of the decay of absorbance at 535 nm (black closed circles) due to ^{3}Ph$_2$Tz* and the rise of absorbance at 380 nm due to BNA$^\bullet$ (red closed circles).

There is no primary isotope effect ($k_H/k_D = 1.00 \pm 0.10$) in the quenching process of ^{3}R$_2$Tz* by BNAH when BNAH is replaced by BNAH-4,4′-d_2 as shown in Figure 10. The k_H values [$(3.6 \pm 0.1) \times 10^9$ M^{-1} s^{-1}, Ph$_2$Tz; $(4.4 \pm 0.2) \times 10^9$ M^{-1} s^{-1}, (ClPh)$_2$Tz; $(4.6 \pm 0.1) \times 10^9$ M^{-1} s^{-1}, Py$_2$Tz in Table 2] agree with those expected from the Gibbs energy relation for the electron-transfer reactions (no. 23, Ph$_2$Tz; no. 24, (ClPh)$_2$Tz; no. 25, Py$_2$Tz blue closed squares in Figure 6a−c).

When BNAH is replaced by 4-*t*-BuBNAH, where the hydrogen at the C(4) position is substituted by a *tert*-butyl group, the photolysis of the Ru(bpy)$_3^{2+}$/Ph$_2$Tz/4-*t*-BuBNAH system results in formation of Ph$_2$Tz$^{\bullet-}$ as detected by ESR (inset of Figure 11). The UV−vis spectral change is shown in Figure 11, where the Ph$_2$Tz absorption band ($\lambda_{max} = 540$ nm) decreases progressively with irradiation time. In this case, electron transfer from 4-*t*-BuBNAH to ^{3}Ph$_2$Tz* occurs to produce 4-*t*-BuBNAH$^{\bullet+}$ and Ph$_2$Tz$^{\bullet-}$, followed by the facile C(4)−C bond cleavage to produce *t*-Bu$^\bullet$ and BNA$^+$ without C(4)−H bond cleavage as shown in Scheme 7. Thus, no overall hydrogen transfer occurs in the case of 4-*t*-BuBNAH, and instead only electron transfer occurs to yield Ph$_2$Tz$^{\bullet-}$.

(58) There is no primary isotope effect in proton transfer from BNAH$^{\bullet+}$ to Ph$_2$Tz$^{\bullet-}$; see Supporting Information S13.
(59) The decay rate of BNA$^\bullet$ obeys second-order kinetics, which corresponds to back hydrogen transfer from Ph$_2$TzH$^\bullet$ to BNA$^\bullet$.
(60) The intercepts, which correspond to the decay rate constants of ^{3}R$_2$Tz*, are slightly different depending on the type of ^{3}R$_2$Tz* (see Supporting Information S4).

Scheme 7

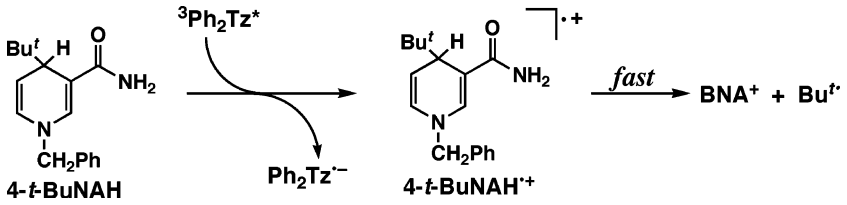

Summary and Conclusions

Efficient energy transfer from $Ru(bpy)_3^{2+*}$ to R_2Tz occurs to produce $^3R_2Tz^*$, which has much longer lifetimes and a higher oxidizing ability than $Ru(bpy)_3^{2+*}$. The reaction of $AcrH_2$ with $^3Ph_2Tz^*$ occurs via one-step hydrogen transfer from $AcrH_2$ to $^3Ph_2Tz^*$, when the deuterium kinetic isotope effect is observed in the rate of hydrogen transfer, which is faster than the predicted rate of electron transfer. When $^3Ph_2Tz^*$ is replaced by $^3(ClPh)_2Tz^*$, which is a stronger acceptor and weaker base than $^3Ph_2Tz^*$, both one-step hydrogen-transfer pathway and the rate-determining electron transfer followed by rapid proton transfer occur competitively. This indicates that the hydrogen-transfer reaction is a mechanistic borderline. The one-step hydrogen-transfer pathway is completely changed to the rate-limiting electron transfer followed by fast proton transfer, when $^3Ph_2Tz^*$ is replaced by $^3Py_2Tz^*$, which is a stronger electron acceptor than $^3Ph_2Tz^*$. In such a case, no deuterium kinetic isotope effect is observed in the rate of overall hydrogen transfer, which agrees with that expected from the free energy relation of the electron-transfer reactions. When $AcrH_2$ is replaced by AcrHPr^i and BNAH, the reactions with $^3R_2Tz^*$ proceed via sequential electron−proton transfer, when the formation of radical cations of AcrHPr^i and BNAH are observed in the laser flash photolysis measurements. The deprotonation from AcrHPr$^{i\bullet+}$ and BNAH$^{\bullet+}$ is retarded as compared with that from $AcrH_2^{\bullet+}$ because of the steric effect of the Pr^i group and the larger pK_a value of BNAH$^{\bullet+}$ than that of $AcrH_2^{\bullet+}$, respectively. In the case of 4-*t*-BuBNAH, the reaction with $^3Ph_2Tz^*$ proceeds via electron transfer followed by the facile C(4)−C bond cleavage. Thus, the reactions of NADH analogues with $^3R_2Tz^*$ occurs via one-step hydrogen transfer, the rate-limiting electron transfer followed by fast proton transfer (fast C−C bond cleavage in the case of 4-*t*-BuBNAH), or sequential electron−proton transfer depending on the electron-donor ability of NADH analogues as well as the electron-acceptor ability of $^3R_2Tz^*$ and the protonation reactivity of $R_2Tz^{\bullet-}$.

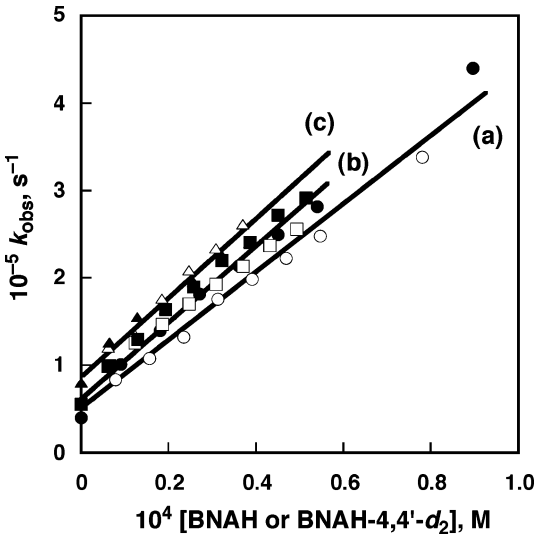

Figure 10. Plots of k_{obs} vs [BNAH] and [BNAH-4,4′-d_2] for the reactions of (a) $^3Ph_2Tz^*$ with BNAH (○) and BNAH-4,4′-d_2 (●), the reactions of (b) $^3Py_2Tz^*$ with BNAH (□) and BNAH-4,4′-d_2 (■), and the reactions of (c) $^3(ClPh)_2Tz^*$ with BNAH (△) and BNAH-4,4′-d_2 (▲) in deaerated MeCN at 298 K.

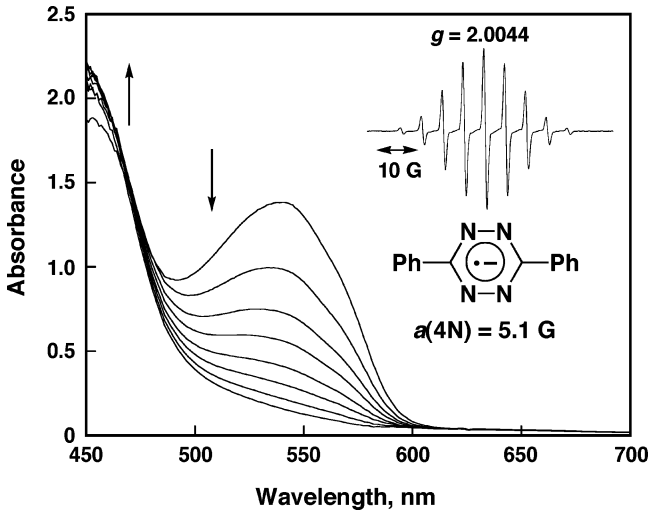

Figure 11. Spectral change observed in the steady-state photolysis of a deaerated MeCN solution of 4-*t*-BuBNAH (1.7×10^{-2} M), Ph_2Tz (2.8×10^{-3} M), and $Ru(bpy)_3^{2+}$ (1.0×10^{-4} M), with monochromatized light of $\lambda = 450$ nm (0−3500 s, 300 s interval) at 298 K. Inset: ESR spectrum of a deaerated MeCN solution containing 4-*t*-BuBNAH (7.3×10^{-3} M) and Ph_2Tz (3.4×10^{-3} M) in the presence of $Ru(bpy)_3^{2+}$ (1.3×10^{-4} M) after photoirradiation with a high-pressure mercury lamp ($\lambda > 400$ nm) at 298 K.

Acknowledgment. This work was partially supported by Grants-in-Aid (No. 16205020) from the Ministry of Education, Culture, Sports, Science and Technology, Japan.

Supporting Information Available: Stern−Volmer plots for the emission quenching of $Ru(bpy)_3^{2+}$ by R_2Tz (S1), decay time profiles of $^3Ph_2Tz^*$ in the absence and presence of O_2 (S2), emission spectra of $^1O_2^*$ (S3), kinetic data for the decay of $^3R_2Tz^*$ (S4), first- and second-order plots for the decay of $^3R_2Tz^*$ (S5), cyclic voltammograms of R_2Tz (S6), Stern−Volmer plots for the emission quenching of $Ru(bpy)_3^{2+*}$ by NADH analogues (S7), absorption spectra of Ph_2Tz and $Ph_2Tz^{\bullet-}$ (S8), transient absorption spectra and the time profiles of $^3(ClPh)_2Tz^*$ and AcrH$^\bullet$ (S9), decay time profiles of AcrH$^\bullet$ and AcrD$^\bullet$ (S10), kinetic data for the back hydrogen-transfer and back electron-transfer processes (S11), the decay time profile of BNAH$^{\bullet+}$ (S12), time profiles of the rise of absorbance due to BNA$^\bullet$ and BNA$^\bullet$-4-d_1 (S13), and transient absorption spectra of $^3Py_2Tz^*$, BNAH$^{\bullet+}$, and BNA$^\bullet$(S14). This material is available free of charge via the Internet at http://pubs.acs.org.

JA0604562